the general science journal

A Luni-Solar Connection to Weather and Climate
II: Extreme Perigean New/Full Moons and El Niño Events

Ian R.G. Wilson*[1] and Nikolay S. Sidorenkov[2]

1. *The Liverpool Plains Day-Time Astronomy Centre Gunnedah, Australia*
2. *Hydrometcenter of Russia, Bolshoy Predtechensky, pereulok, 11-13, 123242 Moscow, Russian Federation, Russia.*

* Address correspondence to this author at email: irgeo8@iinet.net.au

Abstract

Paper I showed that the epochs when the lunar line-of-apse points directly towards/away from the Sun, at times that were closely aligned with the Equinoxes and Solstices (i.e. seasonal boundaries), exhibited distinct periodicities at 28.75, 31.00, 88.50 (Gleissberg cycle), 148.25, and 208.00 (de Vries cycle) years. The caveat being that the alignments had to observed in a frame of reference that was fixed with respect to the Perihelion of the Earth's orbit.

This study expands upon the findings of paper I by showing that the long-term periodicities exhibited by the alignments of the lunar line-of apse with the seasonal boundaries have effectively the same periodicities as the alignments of the Perigean New/Full moons with the seasonal boundaries (provided both are viewed in a frame of reference that was fixed with respect to the Perihelion of the Earth's orbit).

In addition, this study establishes that the very process of selecting the times when the Perigean New/Full moons occur at or near seasonal boundaries, is in fact equivalent to selecting the times when the strongest Perigean New/Full moon tidal events cross the Earth's equator or when they are at their furthest distance from the Earth's equator (i.e. lunar standstill).

The strongest spring tidal events that occur close to either the nominal Vernal Equinox (i.e. 0.00 UT March 21st) or the nominal Autumnal Equinox (i.e. 0.00 UT September 21st) that have peak tides at latitudes that are close to the Earth's equator are selected. Similarly, the strongest spring tidal events that occur close to either the nominal Summer Solstice (i.e. 0.00 UT June 21st) or the nominal Winter Solstice (i.e. 0.00 UT December 21st) that have peak tides at latitudes that are close to those of the lunar standstills are selected, as well.

Collectively, the selected sample shows that the tidal events closest to the Vernal Equinox naturally divides into five 31-year epochs that start in the years 1870, 1901, 1932, 1963, and 1994. The three lunar tidal epochs that start in 1870, 1932, and 1994 begin with a Perigean Full moon, so they are designated as Full Moon epochs. Similarly, the remining two epochs that start in 1901 and 1963 begin with a Perigean New moon, so they are designated as New Moon epochs. In addition, the selected sample shows that the actual starting date for each of the 31-year epochs is dependent upon the specific seasonal boundary that is chosen. The net effect of this is a gradual transition between one lunar epoch and the next that spans a 9.0-year period which is centred upon the time when the strongest spring tide is most closely aligned with the Spring Equinox.

It turns out that the times when strongest tidal peaks cross the Earth's equator [i.e. the Equinox spring tides, which are the strongest spring tidal events that are nearest to the times of the nominal Equinoxes] or the times when the strongest peaks reach their greatest distances from the Equator [i.e. the Solstice spring tides, which are the strongest spring tidal events that are nearest to the times of the nominal Solstices], correspond to the times when the lunar-induced rotational acceleration of the Earth changes sign. This leads to the question, can the tidally induced changes in the sign of the Earth's rotational acceleration be link to an atmospheric/oceanic phenomenon that is known to influence changes in the Earth's global mean temperature? Further investigation shows that the meteorological phenomenon that meets these requirements is the starting dates of moderate to strong El Nino events.

If a comparison is made between the starting dates for moderate to strong El Nino events and the times when the strongest spring tides are near to the Earth's equator [i.e. Equinox spring tides], there is an alignment between the two phenomena during Full Moon epochs (i.e. those starting in 1870, 1932, and 1994). Similarly, if a comparison is made between the starting dates for moderate to strong El Nino events and the times when the strongest spring tides are at their furthest distance from the Earth's equator [i.e. Solstice spring tides], there is an alignment during the New Moon epochs (i.e. those starting in 1901 and 1963).

Hence, we can conclude that, during the Full Moon epochs, there is a significant alignment between the starting dates of moderate to strong El Ninos and the times when Equinox spring tidal events occur and that, during New Moon epochs, there is a significant alignment between the starting dates of moderate to strong El Ninos and the times when Solstice spring tidal events occur. This implies that there must be a connection between the times of strongest Equinox/Solstice spring tidal events and the onset of El Ninos.

Keywords: Gleissberg and de Vries Cycles, Lunar Alignments, Perigean Spring Tides, El Ninos

1. Introduction

Wilson and Sidorenkov (2018 – hereafter paper I) show that the epochs when the lunar line-of-apse points directly towards/away from the Sun, at times that are closely aligned with the Equinoxes and Solstices (i.e. seasonal boundaries), exhibit distinct periodicities at 28.75, 31.00, 88.50, 148.25, and 208.00 years. In addition, this paper notes that these specific periodicities only arise when the close lunar alignments are viewed in a frame of reference that is fixed with respect to the perihelion of the Earth's orbit.

The full significance of this 208.0-year repetition pattern only becomes apparent when the periodicities in these seasonal luni-solar alignments (ϕ) are compared with the periodicities observed in the spectra for two proxy time series. The first series is the amplitude spectrum of the maximum daytime temperatures (T_m) on the Southern Colorado Plateau for the period from 266 BC to 1997 AD (Ron et al. 2012, Salzer and Kipfmueller 2005). The second is the Fourier spectrum of the solar modulation potential (ϕ_m) over the last 9400 years (Abreu et al. 2012, McCracken et al. 2013). Note that ϕ_m is considered to be a proxy index for the changing level of solar activity with time.

When a comparison is made between these three spectra in paper I, it shows that of the nine most prominent peaks in the spectrum of ϕ, eight have matching peaks in the spectrum of ϕ_m, and seven have matching peaks in the spectrum of T_m. Hence, the paper concludes that all three of these phenomena must be related to one another.

A simple heuristic Luni-Solar climate model is developed in paper I in order to explain the connections between ϕ_m and T_m on inter-decadal to centennial time scales. Firstly, the model proposes that there must be some unknown factor associated with the level of solar activity on the Sun (Nef et al. 2001, Svensmark 1998, 2007) that is producing long-term systematic changes in the amount and/or type of regional cloud cover (Laken et al. 2010). Secondly, it further proposes that the resulting changes in regional cloud cover lead to variations in the temperature differences between the tropics and the poles which, in turn, result in changes to the strength of the geostrophic winds (e.g. the zonal tropical winds, Marshall & Plumb 2008). Thirdly, the model argues that it is these changes in the strength of the geostrophic winds that lead to the long-term changes in the poleward energy and momentum flux. And finally, it proposes that it is these changes in flux which governs the rate at which the Earth warms and cools, and hence, determines the long-term changes in the world mean temperature.

The close matches between the periods of the prominent peaks that are seen in spectra of $\boldsymbol{\phi}$ [as opposed to ϕ_m] and T_m in paper I, indicate that a factor that is associated with the epochs when the lunar line-of-apse points directly towards/away from the Sun, at times that are close to seasonal boundaries, must have an influence on the Earth's world mean temperature on inter-decadal to centennial time scales. The Luni-Solar climate model contends that the seasonal luni-solar alignments (i.e. $\boldsymbol{\phi}$) produce long-term periodicities in the strength of the geostrophic wind speeds of the Earth's atmosphere that match those seen in the alignments themselves. The model further proposes that, on inter-decadal to centennial time scales, these zonal changes in wind speed produce similar long-term periodicities in the Earth's mean temperature, through their influence upon the efficiency with which the Earth warms and cools.

This prompts the question: Is there some specific lunar tidal phenomenon that is a short-term counterpart to the seasonal luni-solar alignments that operate on centennial timescales?

Clearly, if such a phenomenon can be identified, it could be used to better understand how the tidal forces influence the Earth's climate.

Section 2 shows that the Perigean New/Full moon tidal cycles that exhibit the least drift (i.e. the best temporal alignment) with respect to the seasons are the closest short-term counterpart to the centennial-scale luni-solar alignments that are discussed in Paper I. The caveat being that the both sets of alignments have to be observed in a frame of reference that was fixed with respect to the Perihelion of the Earth's orbit. The Perigean New/Full moon cycles are the best short-term counterpart because:

a) the Moon is precisely located on the Earth-Sun line when it is New or Full.
b) Perigean New/Full moons occur whenever a New or Full moon takes place at a date that is very close to the Perigee of the lunar orbit.
c) both a) and b) ensure that the Perigee of the lunar orbit is pointing directly towards the Sun at New moon or directly away from the Sun at Full moon.

Section 3 shows that the very process of selecting the times when the Perigean New/Full moons occur at or near seasonal boundaries is in fact equivalent to selecting the times when the strongest Perigean New/Full moon tides either cross the Earth's equator or when they are at their furthest distance from the Earth's equator (i.e. lunar standstill).

In section 4, a comparison is made between the times where the strongest Perigean New/Full moon tidal events cross the Earth's equator and the starting months for all of the moderate to strong El Nino events between 1868 and 2016. This comparison shows that alignment between these two phenomena is highly significant. Finally, the conclusions are summarized in section 5.

2. The Connection Between the Perigean New/Full Moon Cycles and the Centennial-Scale Luni-Solar Seasonal Alignment Cycles.

Figure 1 shows the time difference (in hours) between when a Perigean New/Full moon takes place and the time when it reaches perigee. This time difference is plotted against time in years. The sample of Perigean New/Full moons displayed in this figure is limited to those New/Full moons near perigee that are closer to perigee than the Full/New Moon at perigee that follow them. All Perigean New/Full moons that meet this criterion over the 445-year period from July 18th, 1841 A.D. to September 29th, 2285 A.D are displayed. A positive time difference means that the moon becomes New/Full after it has passed through perigee.

[N.B. The dates and times of perigee are those calculated using the algorithms that are published by Meeus 1998, while the dates and time of the phases of the Moon are those calculated using the algorithms of Meeus 1988. The accuracy and precision of these lunar dates and times are more than enough for the purposes for which they are used in this study (Chapront-Touz, M. and Chapront, J. 1991)].

One example of a Perigean New/Full Moon cycle that is drifting slowly with respect to the seasons is the 31.0-year cycle. This cycle closely aligns with the seasons because 27.5 Full Moon Cycles = 11324.0718 days (= 31.00428 tropical years), 383.5 Synodic months = 11324.9808 days (=31.00677 tropical years) and 411 anomalistic months = 11324.9200 days (= 31.00660 tropical years). This means that if you start out with a Perigean New (/Full) moon at a time when the Perigee of the lunar orbit points directly at (/away from) the Sun then 2.47 days longer than exactly 31.0 tropical years later, you will get a Perigean

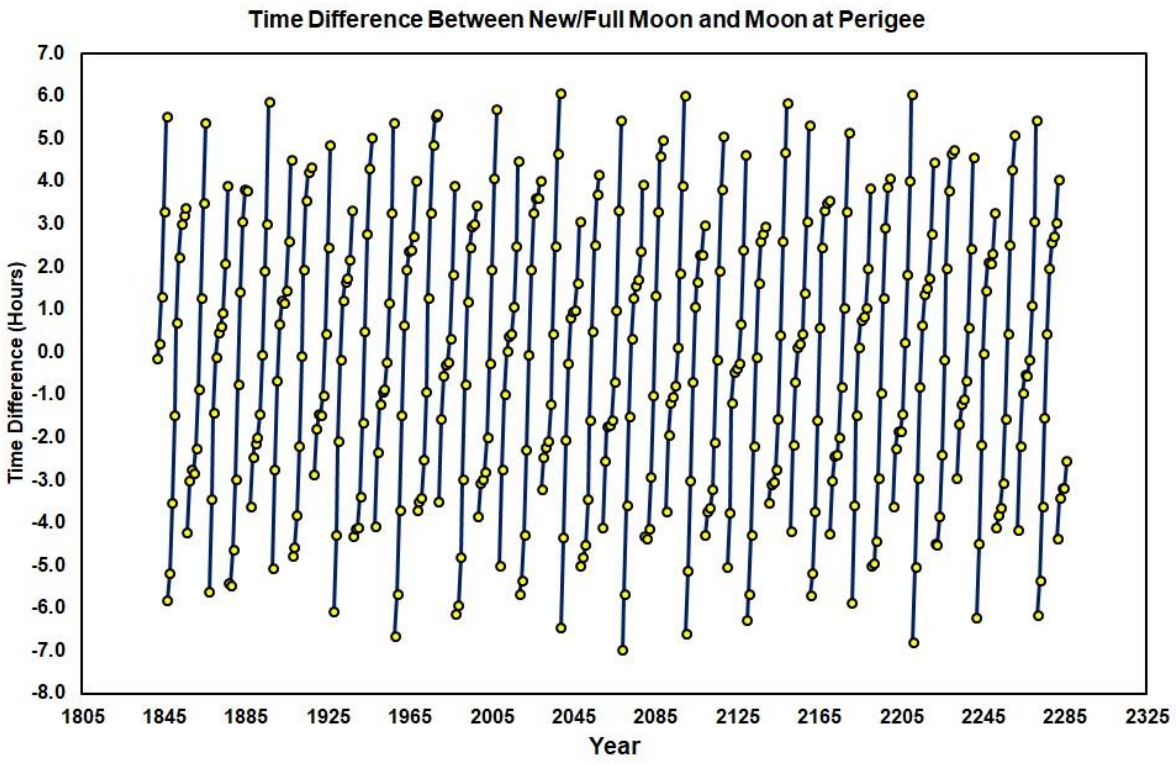

Figure 1

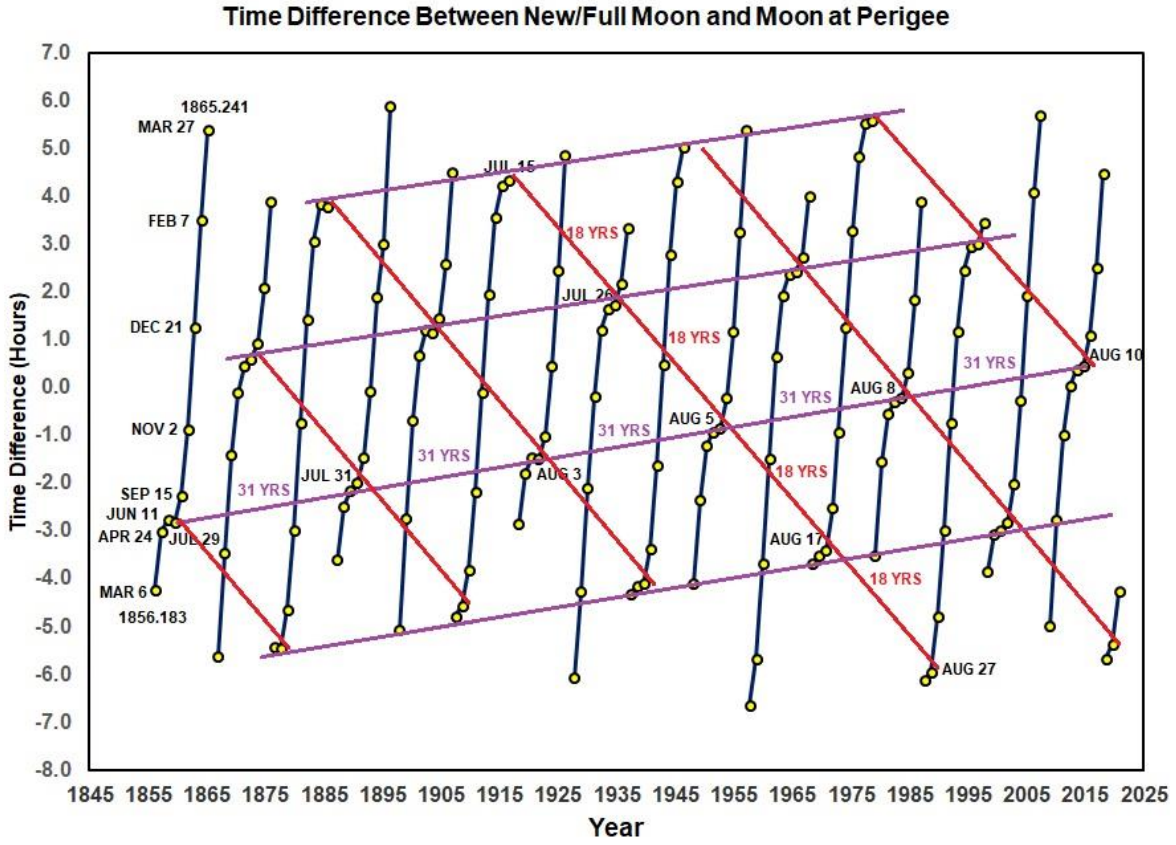

Figure 2

Full (/New) moon that occurs just 0.91 days after the Perigee of the lunar orbit points directly away from (/at) the Sun.

Figure 2 shows a subset of the sample that is displayed in figure 1. This subset spans the period from March 6th 1856 to October 16th 2020. Four examples of the 31.0-year Perigean New/Full moon cycle are highlighted in this figure using four purple straight lines that gradually slope upwards from the lower left towards the upper right. These lines connect Pergiean New (/Full) moons that are separated from an earlier Perigean Full(/New) moon by a period of 31.0 years.

An estimate of the seasonal drift rate can be made using the 31.0-year cycle that is second from the bottom of figure 2. The calendar dates that are placed next to the Perigean New/Full moons in this sequence, show that there are five 31.0-year cycles between July 29th 1859 21:44 U.T. (1859.579) and August 10th 2014 18:11 U.T. (2014.611), producing an average (forward) seasonal drift rate of 2.37 days per 31.00 years (or 0.007 delta years per cycle).

[It is important to note that if you chose any Perigean New/Full moon event in figures 2, one cycle later there will be another event in that cycle. However, after each cycle period, the time difference (in hours) between when the Perigean New/Full moon takes place and the time when it reaches perigee, will slowly drift into and then out of alignment. This can be explained by using the 31.0-year cycle as an example. For this particular cycle, the longest period of time that you can follow the cycle events and still be located within the zone of close alignment (i.e. ± 5 hours), lies somewhere between zero and 434 years (i.e. fourteen cycles), depending upon the misalignment of the first lunar event that is chosen.]

Also shown in figure 2 are six straight red lines that slope downwards from the upper left towards the lower right. These lines connect Perigean New/Full moons that are separated by the 18.030-year lunar Saros cycle. The seasonal drift rate for this cycle can be determined using the 18.030-year cycle that is fourth from the left side of figure 2. The calendar dates that are placed next to the Perigean New/Full moons in this sequence, show that there are four 18.030-year cycles between July 15th 1916 04:40 U.T. (1916.541) and August 27th 1988 10:57 U.T. (1988.657), producing an average (forward) seasonal drift rate of 10.59 days per 18.030 years (or 0.029 delta years per cycle). This tells us that the 18.030-year cycle is not well aligned with the seasons, since it advances through the seasonal year at a rate that is roughly four times that of the 31.0-year cycle. However, it turns out that the 18.030-year Saros cycle is of interest to this study because it interacts with the 31.0-year cycle to form pseudo-cycles that are better aligned with the seasonal calendar.

Figure 3 shows the seasonal drift rates (measured in delta years per cycle) for the 31-year and 18.030-year cycles. These are plotted against the length of the Perigean New/Full moon cycle measured in tropical years. In addition, it shows that the interaction between these two cycles produces a parallel sequence of pseudo-cycles at: (31.0 – 18.0) = 13.0 years; (62.0 – 18.0) = 44.0 years, (93.0 – 18.0) = 75.0 years, and (124.0 – 18.0) = 106.0 years, with each pseudo-cycle separated from its predecessor by 31.0 years.

Figure 2 showed that the dates upon which Perigean New (/Full) moons occur in any given Perigean New (/Full) moon sequence slowly drift through the seasonal calendar, as you move upward along that sequence. In order to highlight the seasonal drift of these events, dates are placed next to the New moons in the first Perigean New moon sequence that starts on March 6th, 1856. These dates reveal that along each of the Perigean New (/Full) moon

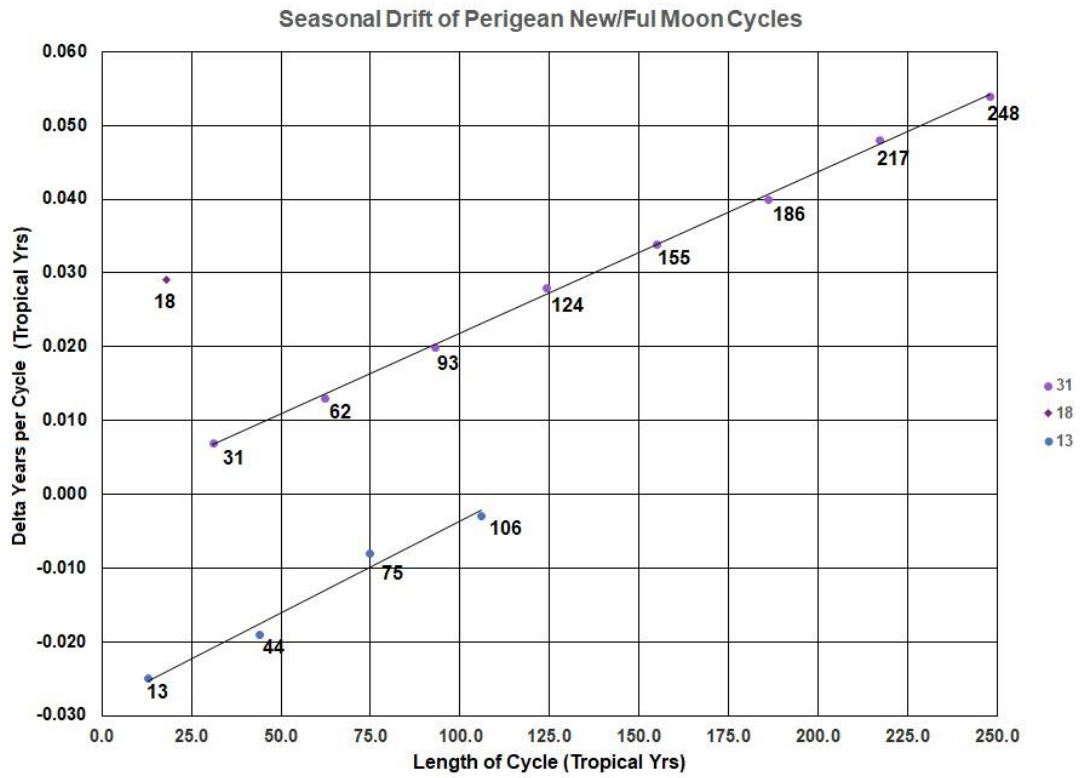

Figure 3

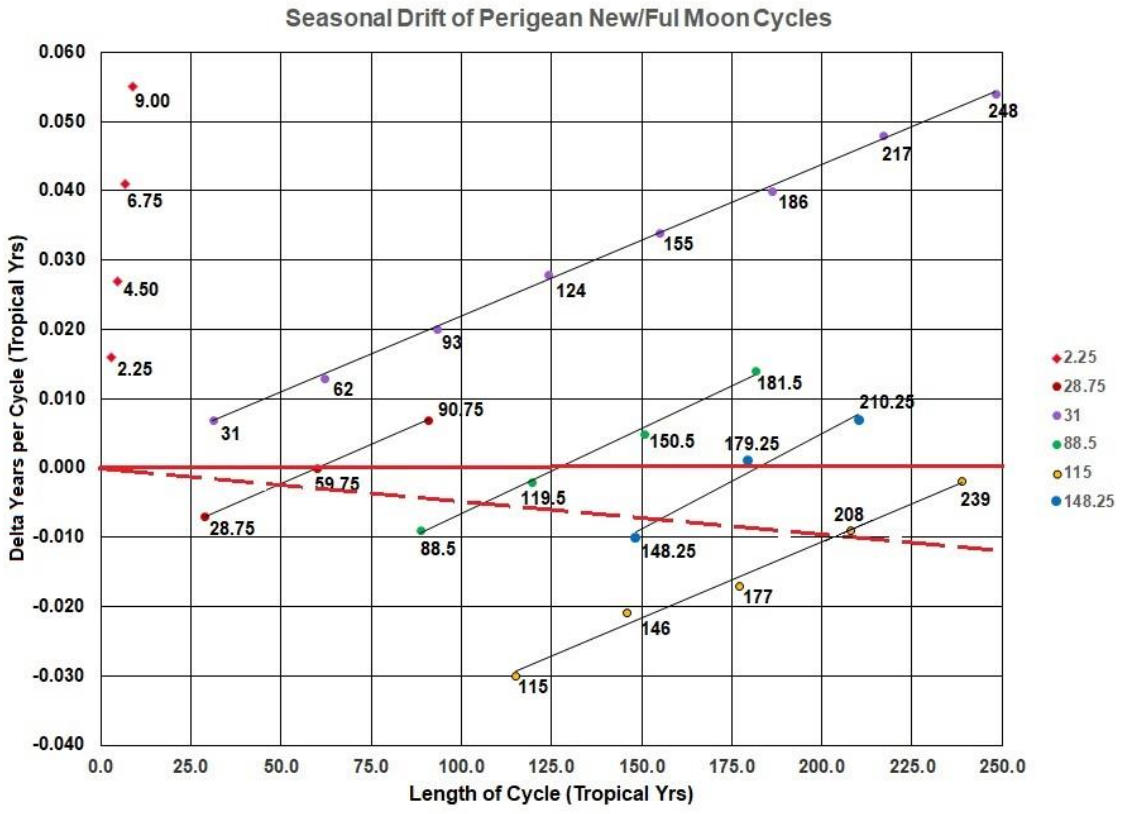

Figure 4

sequences, the repetition cycles that closely align with the seasonal boundaries are at 2.25, 4.50, 6.75, and 9.00 years. These cycles are important because their interaction with 31.0-year cycle lead to pseudo-cycles that account for all the remaining Perigean New/Full cycles in the sample that are closely align with the seasons.

Figure 4 shows all the pseudo-cycles that are generated by the interaction between the 2.25, 4.5, 6.75, and 9.00-year cycles with the 31.0-year cycle. Firstly, the 2.25-year cycle generates the 28.75, 59.75, and 90.75-year pseudo-cycles. Secondly, the 4.50-year cycle generates the 88.5, 119.5, 150.5, and 181.5-year pseudo-cycles. Thirdly, the 6.75-year cycle generates the 148.25, 179.25, and 210.25-year pseudo-cycles, and finally, the 9.00-year cycle generates the 115, 146, 177, 208, and 239-year pseudo-cycles.

In order for a Perigean New/Full moon cycle to be aligned with the seasons, it would have to lie on or close to the red horizontal line in figure 4 [Note that the lunar cycles that are on this line are fixed in a reference frame that is precessing at the same rate as the rotation axis of the Earth]. Figure 4 shows that the cycles that best fit this description are all simple whole multiples of the sum of the 28.75-year and 31.00-year lunar cycles i.e. they are those with periods of 59.75, 119.5, 179.25 and 239.0 years. This means that, on inter-decadal to centennial time scales, the Perigean New/Full moon events that are best aligned with the seasonal calendar reoccur at intervals of 59.75 years, which is very close to 60 years.

Alternatively, if Perigean New/Full moon cycle are viewed in a frame of reference that aligns with the Perihelion of the Earth's orbit, they would lie along the red dashed line in figure 4. The cycles that best fit this description in this figure are the 59.75, 88.5, 148.25 and 208.0-year cycles [N.B. the 119.5-year cycle is just a multiple of the 59.75-year cycle]. These are exactly the same as the periods that were found for luni-solar alignments in paper I, when these alignments were viewed in a frame of reference that was fixed with respect to the Perihelion of the Earth's orbit.

Hence, we have shown that the Perigean New/Full moons reoccur in cycles that show the same periodicities as the luni-solar alignments discussed in paper I, provided both are viewed in a frame-of-reference that is fixed with respect to the Perihelion of the Earth's.

3. Choosing the Perigean New/Full Moon Cycles That are Best Aligned with the Seasonal Boundaries is Equivalent to Selecting the Times When the Strongest Peak Tides Cross the Earth's Equator or When They are Furthest from the Equator.

The yellow tilted elliptical orbits in figure 5, represent the apparent movement of the Sun about the sky as seen from the Earth (i.e. the Ecliptic). The Sun takes a full tropical year (365.2421897 days) to move once about the yellow orbit, crossing the Earth's equatorial plane (the grey plane) once every six months at the Spring and Autumnal (Fall) equinox, respectively.

The red tilted elliptical orbits in this figure, represent the apparent movement of the Moon about the sky as seen from the Earth. The Moon takes a full tropical month (27.321581 days) to move once about the red orbit, crossing the Earth's equatorial plane roughly once every 13.66 days, where the red orbit crosses the black line [N.B. the ~ 5 degrees tilt of the lunar orbit with respect to the ecliptic is ignored as a second order effect for this argument].

Clearly, if the perigee of the lunar orbit points directly towards (/away from) the Sun when they are both very near to the Autumnal/Fall Equinox (i.e. top of figure 5), the Perigean New

(/Full) moons will take place when they are above the Earth's equator on or around September 21st. Similarly, if the perigee of the lunar orbit points directly towards (/away from) the Sun when they are both very near to the Vernal/Spring Equinox (i.e. bottom of figure 5), the Perigean New (/Full) moons will take place when they are above the Earth's equator on or around March 21st.

Figure 6 shows the equivalent situation to figure 5 except that the Perigee of the lunar orbit points directly towards (/away from) the Sun at the time of the Solstices.

In this case, if the perigee of the lunar orbit points directly towards (/away from) the Sun when they are both very near to the Winter Solstice (i.e. top of figure 6), the Perigean New (/Full) moons will take place when they are above their furthest latitudes from the Earth's equator (i.e. at lunar standstills) on or around December 21st. Similarly, if the perigee of the lunar orbit points directly towards (/away from) the Sun when they are both very near to the Summer Solstice (i.e. bottom of figure 6), the Perigean New (/Full) moons will take place when they are above their furthest latitudes from the Earth's equator (i.e. at lunar standstills) on or around June 21st.

Hence, if we select times when Perigean New/Full moons occur at or near seasonal boundaries (which is effectively what we did in paper I), we are in fact selecting times when the strongest tidal events (i.e. the Perigean New/Full moons) are located above specific latitudes on the Earth's surface.

This means that if the Perigee-end of the lunar orbit points directly towards (/away from) the Sun on or around:

a) **June 21st** (i.e. the Summer Solstice), Perigean New (/Full) moons will take place at their furthest points away from the Equator (i.e. at lunar standstills) in the Northern(/Southern) hemisphere.
b) **December 21st** (i.e. the Winter Solstice), Perigean New (/Full) moons will take place at their furthest points away from the Equator (i.e. at lunar standstills) in the Southern(/Northern) hemisphere.

c) **21st of March or the 21st of September** (i.e. the Vernal or Autumnal Equinox, respectively), Perigean New (/Full) moons will take place when these New and Full moons are close to being directly above the Earth's equator.

Confirmation of this is provided by figures 7, 8, 9, 10, and 11.

Ray and Cartwright (2007) have made use of a high precision numerical ephemeris of the Sun and the Moon (DE406) to identify the dates and times of maximum luni-solar tidal potentials (V) for all spring tidal events between the years 1 and 3000 A.D. These authors have calculated each of the peak tidal potentials at a point P on the Earth's surface that are located along a great-circle of arc that lies between the sub-lunar and sub-solar points. They then convert each of these tidal potentials into equilibrium ocean tide heights (i.e. V/g - where g is the acceleration due to gravity = 9.82 ms^{-2}), measured in centimetres.

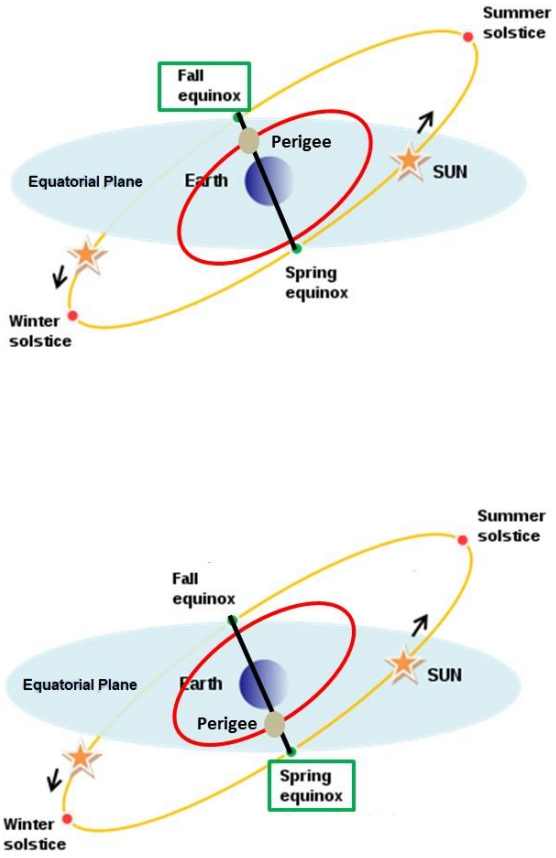

Figure 5

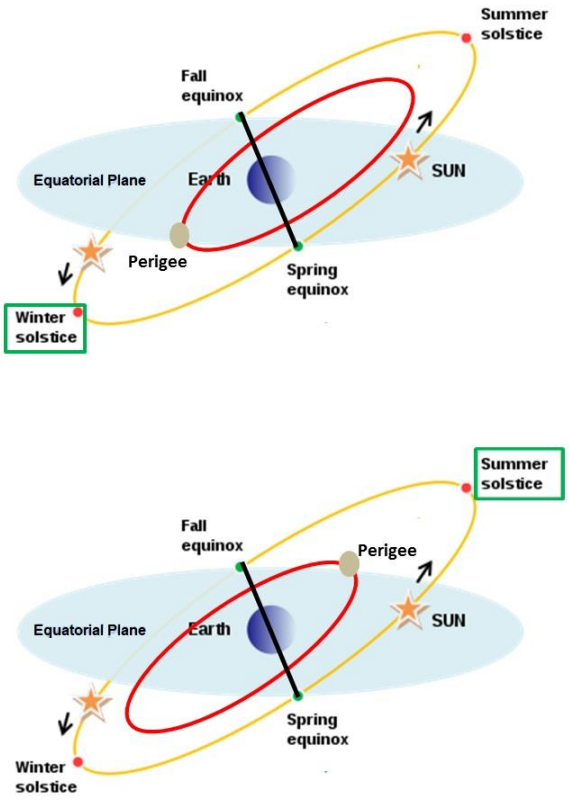

Figure 6

Figure 7 shows the resultant peak equilibrium ocean tidal heights [EOTHs] induced by all the New moon spring tidal events from 1850 to 2020 plotted against the lunar declination at the time of these events. It is important to note that:

1) the fact that the data displayed in these figures represent spring tidal events means that the peak tidal potentials at a point P on the Earth's surface are located at or near the sub-lunar point (and also, by definition, at or very near to the sub-solar point). [N.B. The declination of the Moon at the time of the peak tidal potential differs from the declination of the nearest New or Full moon by less than one degree.]

2) The gradual decrease in the maximum and minimum EOTHs, from the Southern to the Northern Hemispheres, is caused by the ellipticity of the Earth's orbit about the Sun. This results from the fact that the tidal force at the Earth's surface due to the Sun is approximately $1/3^{rd}$ that of the Moon and the fact that the Earth is much closest to the Sun near the Winter Solstice (Perihelion is around January 3^{rd}). Hence, the strongest tidal forces produced by the Perigean New/Full moons near the Winter Solstice (i.e. December 21^{st}) are about 3.3 % stronger than those that are produced by the Perigean New/Full moons near the Summer Solstice (i.e. June 21^{st}).

3) If we were to replot figure 7 for Full rather than New moon spring tidal events, the data point distribution would just be a horizontal reflection about 0^{O} degrees lunar declination.

Appearing as enlarged red dots in figure 7, are all the Perigean New moons from 1850 to 2020 A.D. that are included in the original alignment sample that is displayed in figure 1. As a reminder, this alignment sample includes all the Perigean New/Full moons that are closer to perigee than the Perigean Full/New moons that follow them. The Perigean New/Full moons that are in this alignment sample are the ones that reoccur in periodic cycles that show the same periodicities as the long-term luni-solar alignments discussed in paper I (provided both are viewed in a frame-of-reference that is fixed with respect to the Perihelion of the Earth's).

Figure 7 and its Full moon equivalent show that the spring tides produced by the Perigean New/Full moons in the original alignment sample are amongst the strongest of those that can occur at latitudes where the Moon appears directly overhead (i.e. from 28.6^{O} south to 28.6^{O} north).

Figure 8 is a reproduction of figure 7. However, in this figure the enlarged red dots highlight all the Perigean New moons that occur within ± 15 days of either the Vernal (March 21.0) or Autumnal Equinox (September 21.0). Similarly, the enlarged yellow dots highlight all the Perigean New moons that occur between ± 15 days and ± 30 days of Equinoxes. [N.B. As with figure 7, if we were to replot figure 8 for Full rather than New moon spring tidal events, the data point distribution would just be a horizontal reflection about 0^{O} degrees lunar declination].

Figure 9 shows the resultant peak EOTHs induced by all the New moon spring tidal events from 1850 to 2020 plotted against the longitude of the Perigee of the lunar orbit at the time of these events. The enlarged red and yellow dots in figure 9 are highlighted for the same reasons as those in figure 8. [N.B. If we were to replot figure 9 for Full rather than New

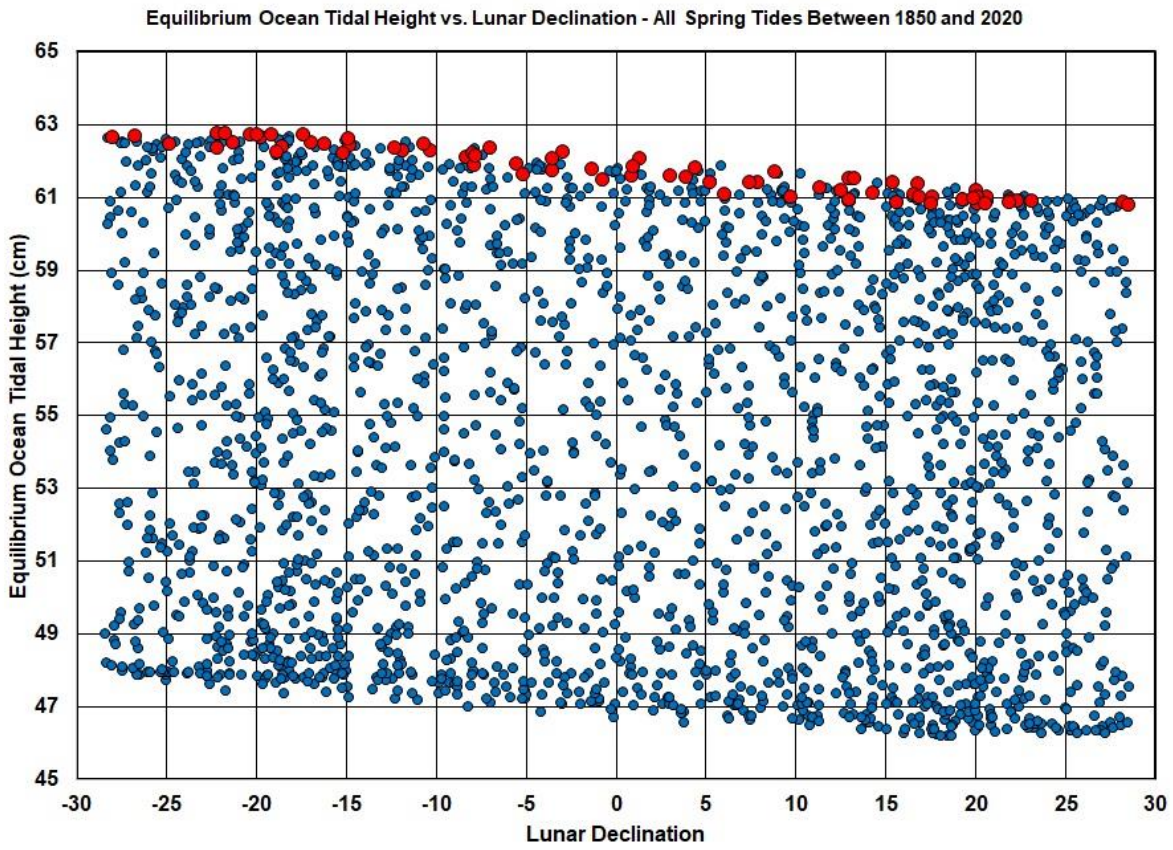

Figure 7

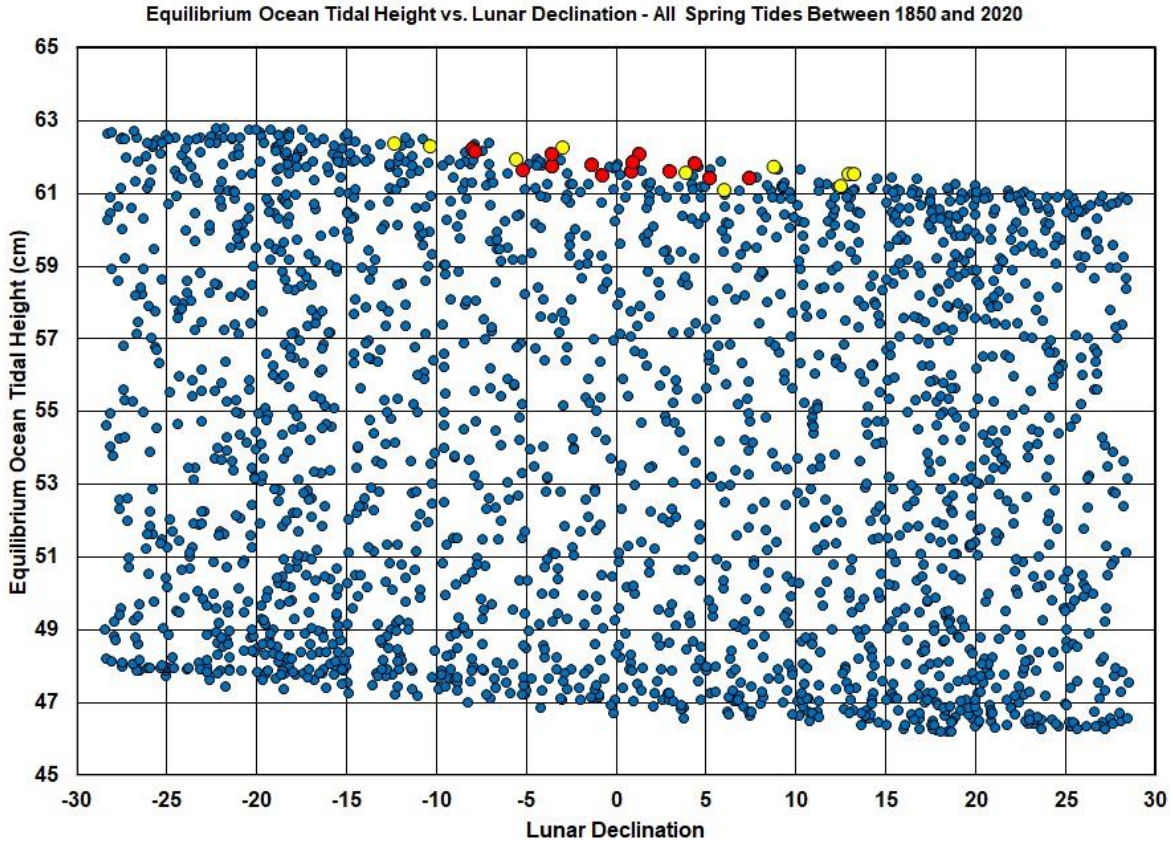

Figure 8

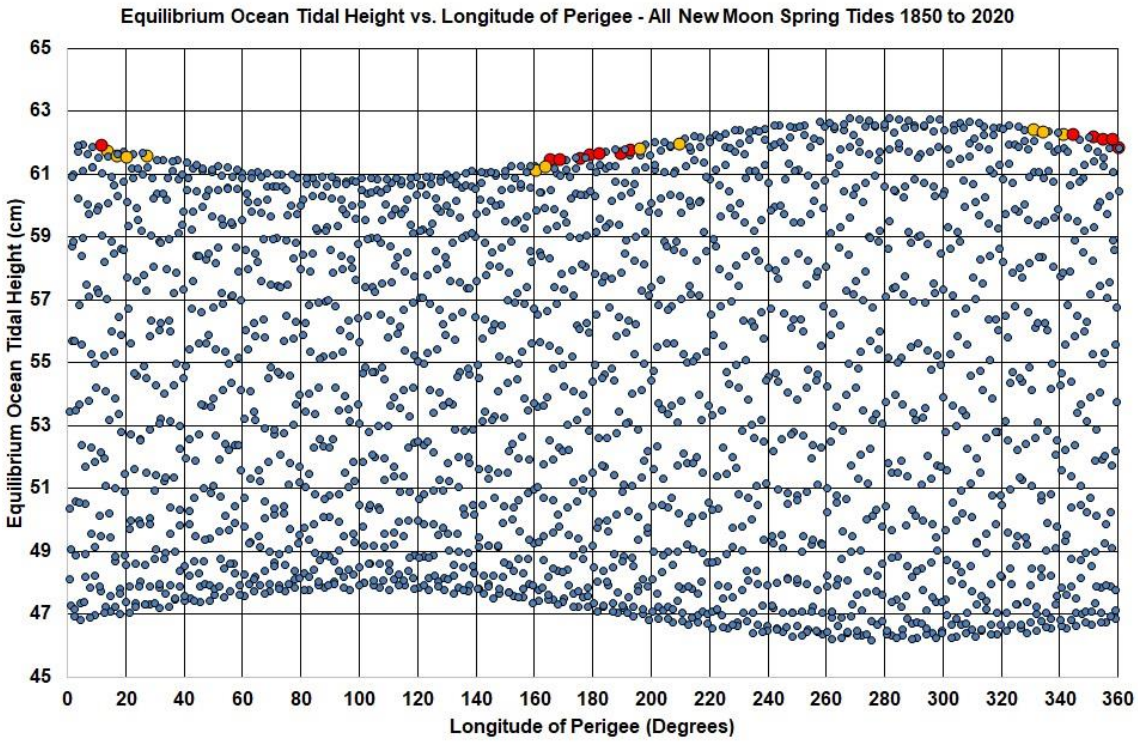

Figure 9

moon spring tidal events, the data point distribution would just be a simple horizontal reflection about a longitude of perigee of 180^{O}].

What the highlighted data points in figures 8 and 9 tell us is that when the Perigee of the lunar orbit points at the Sun around the Vernal equinox (i.e. when the longitude of the perigee of the lunar orbit equal 0^{O} on March 21st) and the Autumnal equinox (i.e. when the longitude of the perigee of the lunar orbit equal 180^{O} on September 21st), the extreme tides produced by the Perigean New (/Full) moons in the original sample (displayed in figure 1) occur when their respective sub-lunar points are at or very near to the Earth's equator.

Figure 10 shows another reproduction of figure 7. In this figure, the enlarged red dots in this figure highlight all of the Perigean New moons that occur within ± 30 days of either the Summer (June 21.0) or Winter Solstice (December 21.0). In addition, figure 11 shows the resultant peak EOTHs induced by all of the New moon spring tidal events from 1850 to 2020, plotted against the longitude of the Perigee of the lunar orbit at the time of these events. The enlarged red dots in figure 11 are highlighted for the same reasons as those in figure 10.

What the highlighted data points in both figure 10 and 11 tell us is that when the Perigee of the lunar orbit points at the Sun around the Summer Solstice (i.e. when the longitude of the perigee of the lunar orbit equal 90^{O} on June 21st) and the Winter Solstice (i.e. when the longitude of the perigee of the lunar orbit equal 270^{O} on December 21st), the extreme tides produced by the Perigean New (/Full) moons in the original sample (displayed in figure 1) occur when their respective sub-lunar points are at or very near their furthest points from the Earth's equator (i.e. at the time of a lunar standstill).

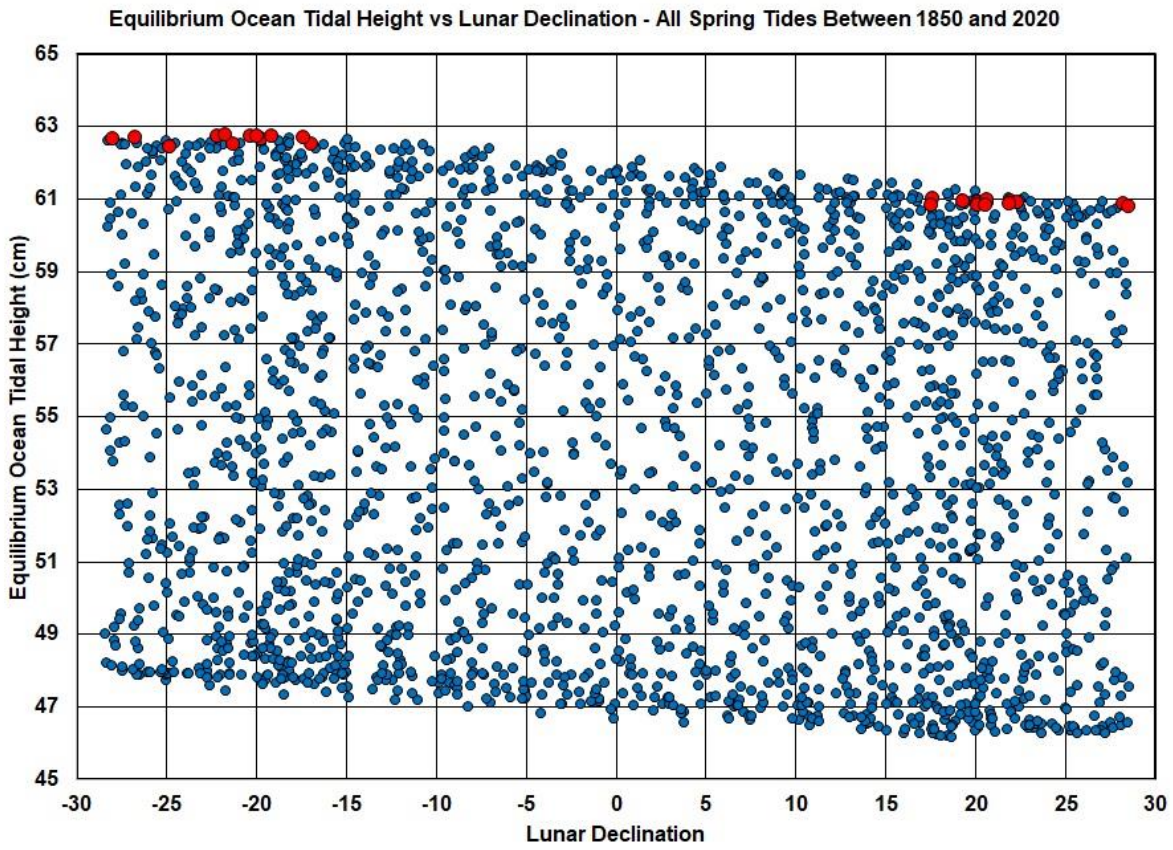

Figure 10

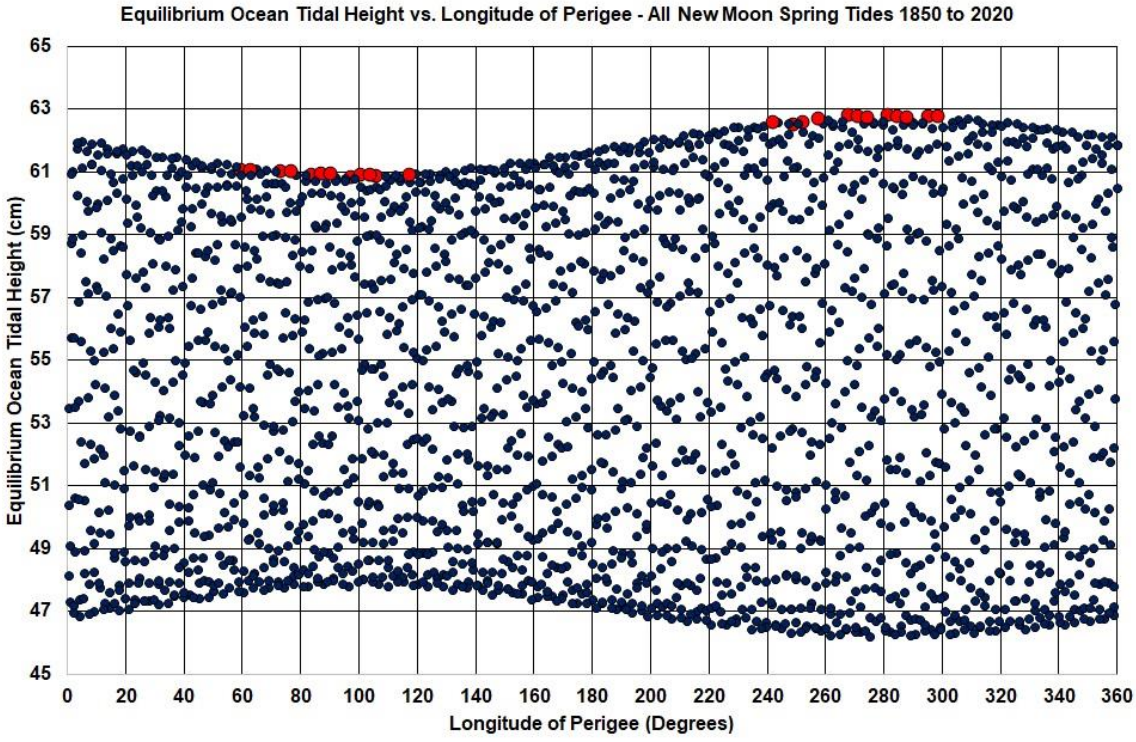

Figure 11

Hence, figures 7 through 11 collectively show that the long-term (inter-decadal to centennial) cycles in the times when Perigean New/Full moons align with the seasonal boundaries are directly connected to a very specific set of short-term (i.e. sub-decadal) lunar tidal cycles. These cycles are those that are associated with the times when the strongest Perigean New/Full moon tidal events cross the Earth's equator (hereafter referred to as the Equinox spring tides) or when these extreme tidal events occur at their greatest distances from the Equator (hereafter referred to as the Solstice spring tides).

It turns out that the one thing that links the times when tidal peaks cross the Earth's equator with the times when these peaks reach their greatest distances from the Equator, is that they both correspond to the times when the lunar-induced rotational acceleration of the Earth changes sign. This leads to the question, can these lunar induced changes in the sign of the Earth's rotational acceleration be link to any atmospheric/oceanic phenomenon that is known to influence changes in the Earth's global mean temperature?

The next section shows that the onset times for El Nino events meets these specific requirements. The link is established through a comparison between, the times when the Equinox spring tides produce the largest EOHTs near the Earth's equator, and the onset times for historical El Nino events.

4. Evidence that Moderate to Strong EL Nino Events are Triggered by Lunar Tides

a) Times when the Equinox spring tides produce the largest EOTHs near the Earth's equator

Figure 12 shows fractional part of a year versus the year for all the spring tides that occurred between March 7th 1860 and March 11th 2030 that have:

1) EOTH's $\geq$ 60.00 cm.
2) tidal peaks which take place within $\pm$ 6^{O} of the Earth's equator.

The selection criteria have been chosen in order to pick out the strongest spring tides that occur close to the Vernal Equinox (i.e. 0.00 UT March 21st) which have peak EOTH's at latitudes that are close to the Earth's equator (i.e. $\leq$ 6.0^{O}). In order to highlight the strongest of these tides, all spring tides in figure 12 with EOTH's $\geq$ 60.67 cm are displayed as large red dots, while all those with EOTH's < 60.67 cm are displayed as small blue dots. In addition, five extra spring tidal events have been added to the sample in figure 12. These spring tides have sub-lunar points at latitudes that are just outside the 6^{O} limit (i.e. with latitudes between 6.0^{O} and 6.4^{O}) and EOTH's $\geq$ 60.67 cm. These purpose of adding these extra five data points is to show the effects of slightly varying the chosen latitude limit.

Figure 13 is the corresponding plot to that of figure 12, except that it shows all of the strongest peak tides that occur close to the Autumnal Equinox (i.e. 0:00 UT September 21st). The meaning of the symbols used in this figure are the same as those for the data points in figure 12.

Finally, figure 14 is a combined plot of all the data points in figure 12 and 13, with the points from figure 13 moved backward in time by 184 days (= 0.5038 years, Bromberg 2016 and GreenwichMeanTime.com 2019) so that the Autumnal equinox is shifted to roughly

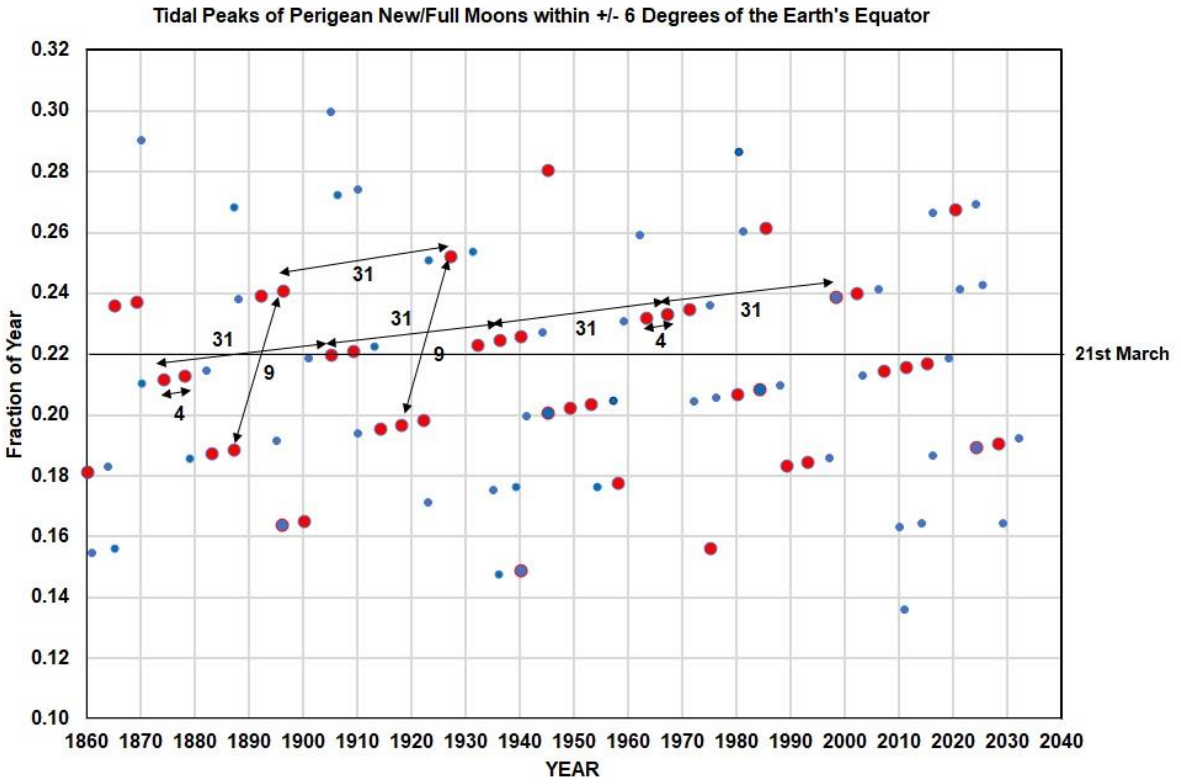

Figure 12

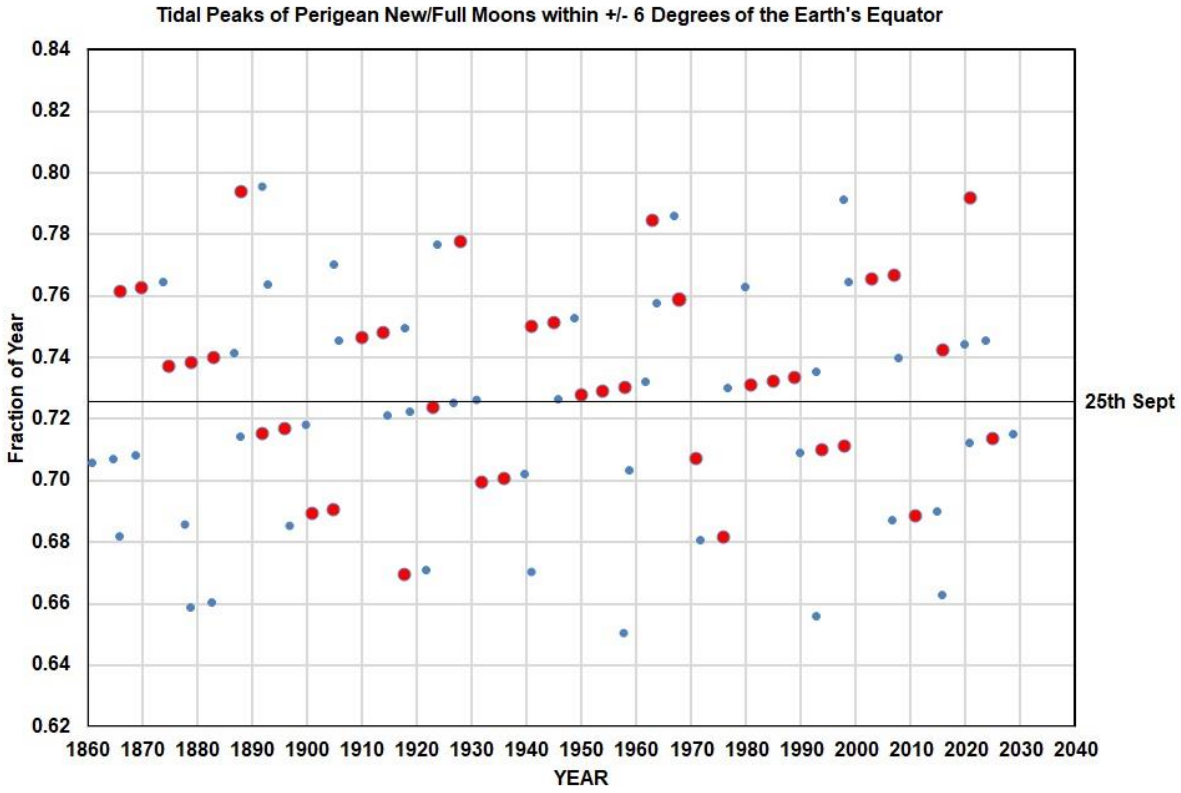

Figure 13

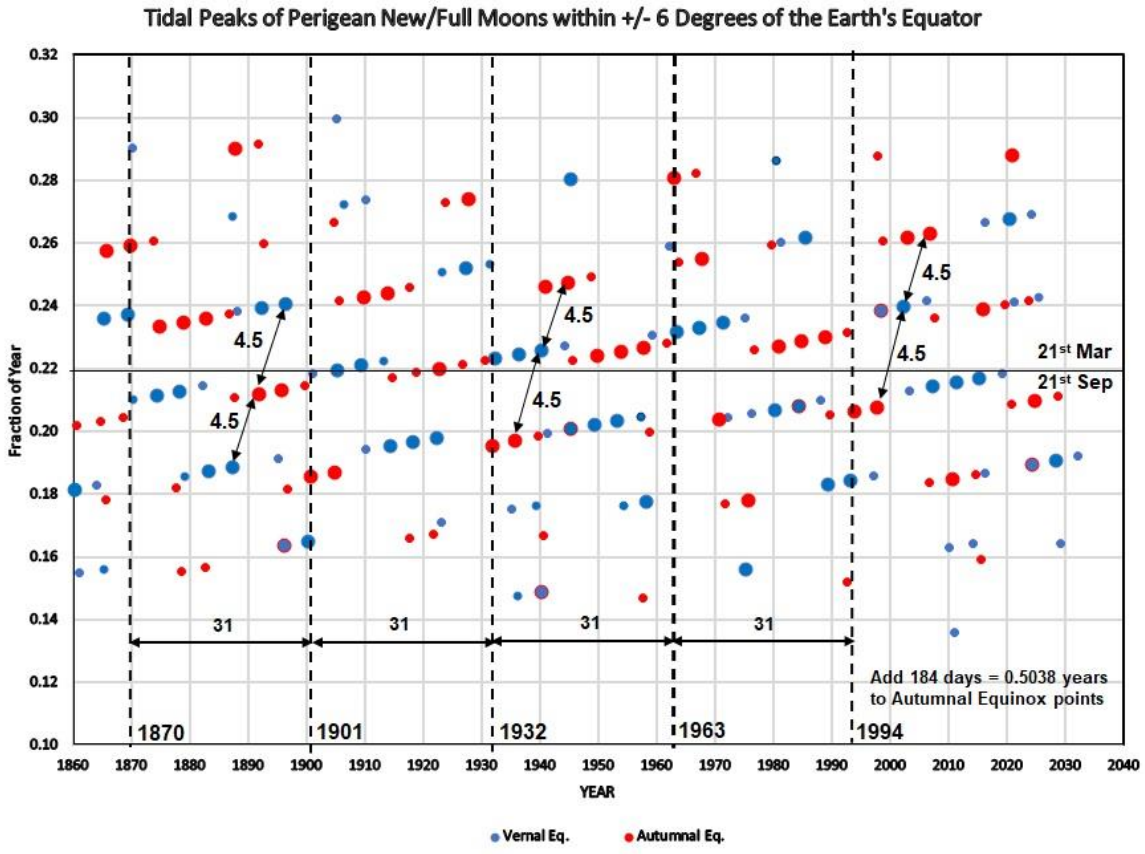

Figure 14

coincide with the Vernal equinox. Note that in figure 14, spring tides that are close to Vernal Equinox are displayed as blue dots while spring tides that are close to the Autumnal Equinox are displayed as red dots.

The spring tides in both figure 12 and 13 show:

1) clusters of four or five data points that are separated from each other by 31.0 years, as you move from left to right across these diagrams.
2) data points within a cluster group alternate between New and Full moon spring tides, with each separated from its predecessor by 4.0 years.
3) clusters of data points that are separated by 9.0 years, as you move from the bottom towards the top of the diagrams.

As an aside, it is important to note that combinations of the 9.0 and 31.0 repetition pattern that are seen in figures 12 and 13 naturally produce the 208-year de Vries pseudo-cycle since (7 x 31) – 9 = 208 years (Damon and Sonnet 1991).

Figure 14 shows that if you look at the clusters of spring tides between 1870 and 1994 that are the closest to the Vernal/Autumnal Equinoxes (i.e. those with a fractional year closest to 0.220/0.724 years), you find that they exhibit a natural repetition pattern of 31.0 years, as you move from left to right across the diagram. This pattern consists of four strong spring tides that are close to the Vernal Equinox, spanning a total of 12 years, a 1 ½ year gap, five strong

Table 1

Epoch	Year	Date	Time (U.T.)	Diff. (dy:hr:min)	Lat (o)	Dist. (km)	EOTH (cm)	Phase (N/F)
1	1870.210	Mar 17	18:46	-03:05:14	4.20	358634	61.302	F
2	1901.219	Mar 20	18:12	-00:05:48	4.69	358799	61.216	N
3	1932.223	Mar 22	17:27	+01:17:27	-2.60	358560	61.388	F
4	1963.232	Mar 25	16:39	+04:16:39	-1.58	358508	61.265	N
5	1994.237	Mar 27	16:03	06:16:03	-7.16	358293	61.362	F

spring tides that are close to the Autumnal Equinox, spanning a total of 16 years, and another 1 ½ year gap (such that 12 + 1 ½ + 16 + 1 ½ years = 31 years).

In addition, figure 14 shows that the starting years for the five 31-year epochs that are associated with the strongest spring tides that closely align with the Vernal equinox are 1870, 1901, 1932, 1963 and 1994. For visual effect, the dates for the spring tidal events that mark the beginning of the five epochs are shown as vertical dashed lines in figure 14. The actual dates are displayed in Table 1, as well.

Three of the lunar tidal epochs that start in 1870, 1932, and 1994 begin with a Perigean Full moon, so they are designated as Full Moon epochs. In like manner, the remining two epochs that start in 1901 and 1963 begin with a Perigean New moon, so they are designated as New Moon epochs. The reason for making a distinction between New and Full moon epochs will become apparent later in this investigation.

Finally, figure 14 shows that there is a natural repetition pattern between clusters of 4.5 years, as you move from the bottom to the top of the diagram. Again, it is important to point out that combinations of the 4.5 and 31.0 repetition patterns that are seen in this figure naturally produce the 88.5-year Gleissberg cycle (Gleissberg 1944, Peristykh and Damon 2003) since (3 x 31) – 4.5 = 88.5 years.

b) Times when the Solstice spring tides produce the largest EOTHs close to lunar standstills.

Figure 15 shows fractional part of a year versus the year for all the spring tides that occurred between December 1st 1861 and December 14th 2031 that have:

1) EOTH's ≥ 60.00 cm.
2) tides that peak within 3^{O} of the latitude of the nearest lunar standstill.

These selection criteria are chosen in order to pick out the strongest spring tides that occur close to either the Summer Solstice (i.e. 0:00 UT June 21st = 0.473 years) or the Winter Solstice (i.e. 0:00 U.T. December 21st = 0.975 years). As a way of further highlighting the strongest tides, all spring tides in figure 15 with EOTH's ≥ 60.67 cm are displayed as large red (Summer Solstice) or large blue (Winter Solstice) dots, while all those with EOTH's < 60.67 cm are displayed as small red or blue dots, respectively. Finally, it is important to note that the Summer solstice points plotted in figure 15 have been shifted forward in time by 182 days (= 0.4983 years, Bromberg 2016 and GreenwichMeanTime.com 2019) so that the

Table 2

Epoch	Year	Date	Time (U.T.)	Diff. (dy:hr:min)	Lat (o)	Dist. (km)	EOTH (cm)	Phase (N/F)
1								
Autumn	1865.682	Sep 05	21:31	-15:02:29	-2.19	360401	60.077	F
Winter	**1867.947**	Dec 11	18:27	**-09:05:33**	18.42	359288	61.59	F
Spring	**1870.210**	Mar 17	18:46	**-03:05:14**	4.20	358634	61.302	F
Summer	**1872.471**	Jun 21	11:58	**+00:11:58**	-25.28	358788	60.343	F
Autumn	**1874.737**	Sep 26	3:20	**+05:03:20**	0.64	358446	61.154	F
2								
Autumn	1896.685	Sep 07	7:41	-13:12:19	2.01	360439	60.121	N
Winter	**1898.953**	Dec 13	17:58	**-07:06:02**	-24.58	359464	61.659	N
Spring	**1901.219**	Mar 20	18:12	**-00:05:48**	4.69	358799	61.216	N
Summer	**1903.483**	Jun 25	11:06	**+04:11:06**	18.36	358791	60.224	N
Autumn	**1905.745**	Sep 29	2:31	**+08:02:31**	-0.21	358466	61.145	N
3								
Autumn	**1927.698**	Sep 11	19:49	**-09:04:11**	-7.71	359954	60.218	F
Winter	**1929.961**	Dec 16	17:09	**-04:06:51**	27.13	359013	61.784	F
Spring	**1932.223**	Mar 22	17:27	**+01:17:27**	-2.60	358560	61.388	F
Summer	**1934.489**	Jun 27	10:20	**+06:10:20**	-25.99	358587	60.386	F
Autumn	**1936.749**	Oct 01	1:45	**+10:01:45**	8.66	358068	61.245	F
4								
Autumn	**1958.704**	Sep 13	19:14	**-07:04:46**	-0.13	360171	60.257	N
Winter	**1960.964**	Dec 18	16:39	**-02:02:21**	-18.75	359034	61.728	N
Spring	**1963.232**	Mar 25	16:39	**+04:16:39**	-1.58	358508	61.265	N
Summer	**1965.494**	Jun 29	9:23	**+08:09:23**	25.38	358721	60.357	N
Autumn	1967.759	Oct 04	1:07	+13:01:07	-3.83	358334	61.291	N
5								
Autumn	**1989.709**	Sep 15	18:16	**-05:05:44**	1.13	359742	60.456	F
Winter	**1991.974**	Dec 21	16:03	**+00:16:03**	24.08	358851	61.933	F
Spring	**1994.237**	Mar 27	16:03	**06:16:03**	-7.16	358293	61.362	F
Summer	**1996.498**	Jul 01	8:31	**+10:08:31**	-17.97	358256	60.427	F
Autumn	1998.764	Oct 06	0:12	+14:00:16	2.56	357910	61.432	F

Summer Solstice data is moved to coincide with the Winter Solstice data. [N.B. Seven extra spring tidal events have been added to the sample in figure 15. These spring tides have sub-lunar points at latitudes that are just outside the 3^{O} limit and EOTH's $\geq$ 60.67 cm. These purpose of adding these extra seven data points is to show the effects of slightly varying the chosen latitude limit].

As with figure 14, the strongest spring tides that align with the Summer Solstice shown in figure 15 naturally breaks up into five consecutive 31-year epochs with starting dates in the years 1872, 1903, 1934, 1965, and 1996. These dates are displayed as vertical dashed lines in figure 15 and they are listed in Table 2, as well.

A comparison between figures 14 and 15 shows that the actual starting date for each of the 31-year epochs is dependent upon the seasonal boundary that is chosen. Table 2 shows the starting dates that would apply for the five epochs, for each of the seasonal boundaries (i.e.

Figure 15

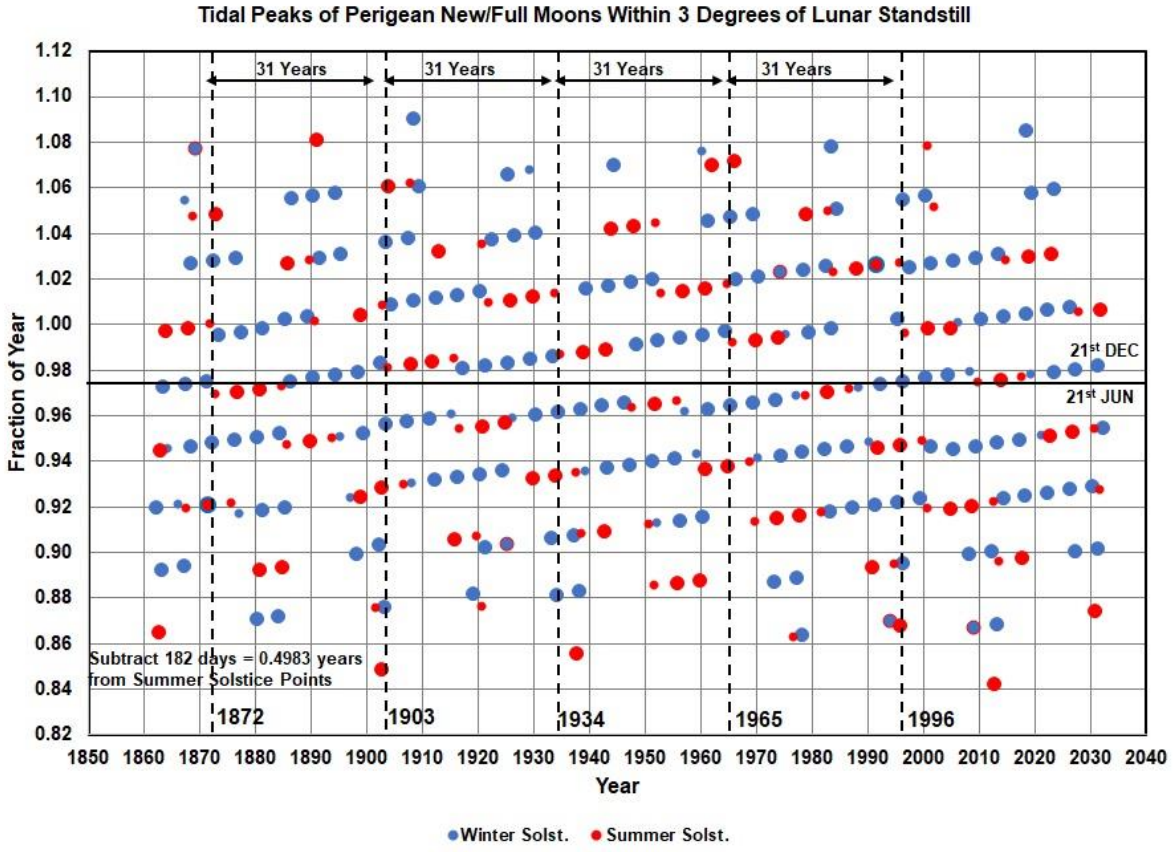

Figure 16

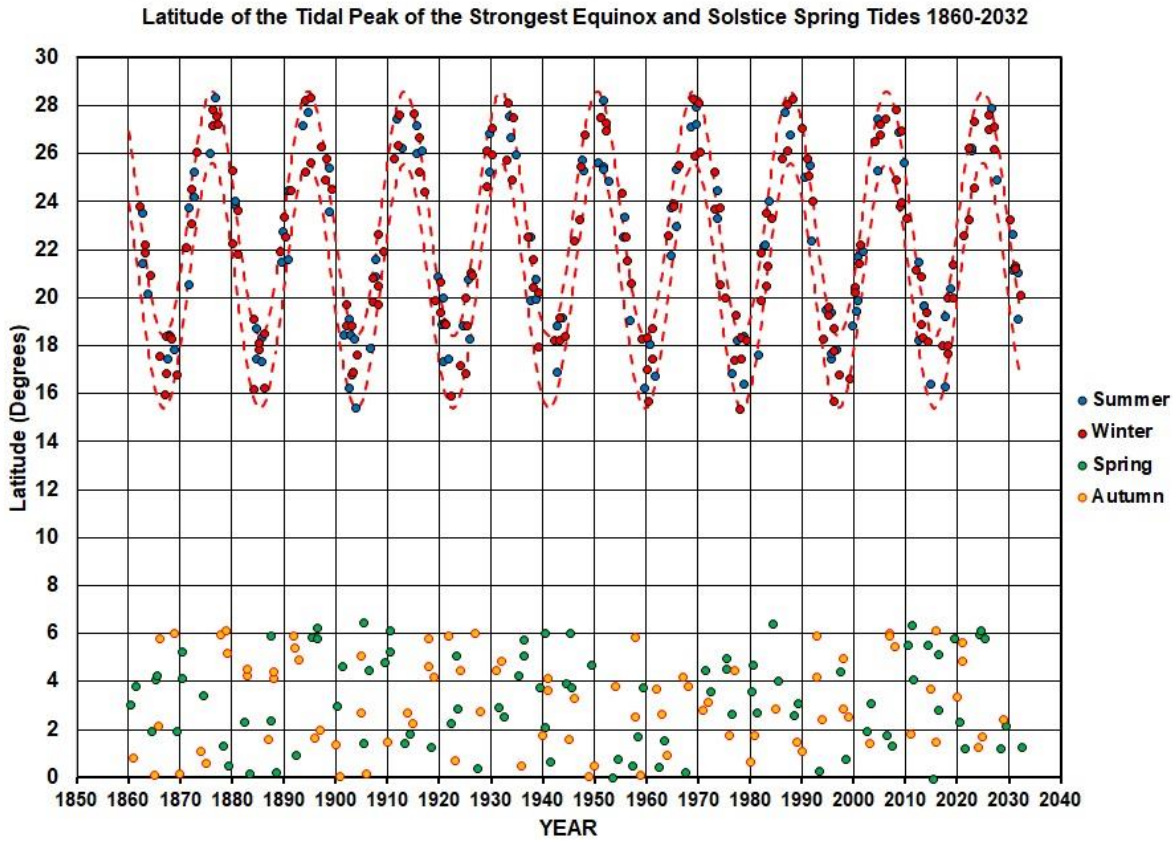

the Autumnal and Vernal Equinoxes and the Summer and Winter Solstices). The data in table 2 shows that there is in fact a gradual transition between one lunar epoch and the next that spans a 9.0-year period that is centred upon the time when the strongest spring tide is most closely align with the Spring Equinox. Table 2 lists these spring tidal events.

Column 5 of table 2 shows the time difference (in days, hours and minutes) between the spring tidal event that marks the boundary between two epochs and their nearest seasonal boundary (which nominally takes placed on the 21st of the month at 0:00 UT). It is clear from this table that the sequence of transitional spring tidal events slowly drifts into and then out of alignment with the nominal seasonal boundaries. This means that the end of the epoch that starts in 1994.237 is not in 2025.243 (i.e. 31-year later – see table 2) as the spring tidal events would no longer be in close alignment with the seasonal boundaries. The most likely outcome is that epoch boundary marked by the strongest spring tidal events that align with the Spring Equinox near 2025.243 (i.e. March 29th 15:15 UT 2025) would move back in time by 4.531 years to a new epoch boundary marked by the strongest spring tidal events that align with the Autumnal Equinox near 2020.712 (i.e. September 17th 17:33 U.T. 2020). This would produce a series of 31-year epochs (starting with strong spring tides that are aligned with the Autumnal Equinox) in the years 2020, 2051, 2082, 2113, and 2144 that closely match the series of 31-year epochs (starting with strong spring tides that are aligned with the Spring Equinox) in the years 1870, 1901, 19 32, 1963, and 1994.

Finally, figure 16 shows the absolute latitudes of the tidal peaks associated with the strongest Equinox and Solstice aligned spring tides between 1860 and 2032. The Solstice aligned spring tides fall between the absolute latitudes of the lunar stand stills (represented by the top red dotted sinusoidal line) and the absolute latitude that is 3.0^{O} less than this (represented by the bottom red dotted sinusoidal line). Similarly, the Equinox aligned spring tides fall between the Earth's Equator (0^{O} latitude) and 6^{O} absolute latitude.

The next step is to establish the onset times for historical El Nino events so that they can be compared to the times of the times of the strongest spring tides that are best aligned with the Equinoxes and the Solstices (figures 14 and 15).

c) The onset times for historical El Nino events

The El Nino is part of a coupled atmospheric and oceanic climate phenomenon known as the El-Nino Southern-Oscillation (ENSO). Traditionally, either an atmospheric based metric called the Southern Oscillation Index (SOI, NOAA 2019a) or a sea-surface temperature-based metric called the Nino3.4 SST anomaly index (NOAA 2019b) is used to determine if El Nino conditions exist in the eastern and central Equatorial Pacific Ocean. However, there is an enhanced ENSO metric that effectively combines the atmospheric information (i.e. the SOI index) with the oceanic information (i.e. the Nino3.4 SST anomaly) about the ENSO. This metric is known as the Bivariate ENSO Time series (BEST) index [Smith and Sardeshmukh 2000 and 2018a].

The first step in the creation of BEST index is to remove the monthly mean climatology for the period 1898 – 2000 from both the SOI and Nino 3.4 SST anomaly indices. After that, the values are standardized by the month so that each month has a mean of 0 and a standard deviation of 1.0, for all years during the output time period. Next, the resulting SST and SOI values are averaged for each month of the time series. Finally, either a 3- or 5-month running mean is applied to both time series [Smith and Sardeshmukh 2018b].

Smith and Sardeshmukh (2018c) present a table that lists all the months where the SST index exceeds 1.28 standard deviations above the mean for that given month and the SOI index exceeds 1.28 standard deviations below the mean for the same month. The months that met this selection criterion were determined for the data that cover the years from 1870 to March 2018. In addition, Smith and Sardeshmukh (2018d) present a slightly less stringent list of El Nino months (covering the period from 1870 to March 2018) that uses 0.96 standard deviation cut-off rather than 1.28.

The less stringent criteria of Smith and Sardeshmukh is adopted for our El Nino sample to maximize the number of El Nino events available for statistical analysis. In addition, since some of the weaker El Nino events could be triggered by stochastic processes within the ENSO climate system itself, the final El Nino sample is limited to those El Nino events that last for more than three months. This is done in order to minimize the level of contamination of the sample through the inclusion of marginal events. Table 3 shows the dates for the starting month for all the El Nino Events that take place between January 1870 and March 2018 that meet the stated selection criteria given.

d) A comparison between the onset times for El Nino events and the strongest Equinox and Solstice spring tides.

Figure 17 shows the time difference in years (column 7 of table 3) between the starting date for each El Nino event (columns 1 – 3 of table 3) and the dates for the strongest Equinox spring tides that occur immediately before and after the start of that event (column 5 and 6 of table 3, respectively). The reader is reminded that the Equinox spring tides referred to here are those that are closet to the dates of the nominal equinox that are displayed in figure 14. [N.B. An "E" in column 4 of table 3 indicates that the starting date for an El Nino event is being compared with dates of the Equinox spring tides, while an "S" in column 4 indicates that the starting date is being compared with dates of the Solstice spring tides].

Figure 18 shows the time difference in years (column 7 of table 3) between the starting date for each El Nino event (columns 1 – 3 of table 3) and the dates for the strongest Solstice spring tides that occur immediately before and after the start of that event (column 5 and 6 of table 3, respectively). Again, the reader is reminded that the Solstice spring tides referred to here are those that are closet to the dates of the nominal solstice that are displayed in figure 15. Of course, the four-year spacing between both strong Equinox and Solstice spring tidal events means that the largest possible absolute time difference that can be plotted in figures 17 and 18 is 2.0 years. In addition, it is important to note that in the case of the 1902, 1957, 1977, and 1987 El Nino events there is some ambiguity as to whether the summer or winter Solstice spring tidal sequence should be used. This ambiguity is resolved by choosing the Solstice spring tide with the strongest Equilibrium Ocean Tidal Height (EOTH) that is closets to the start of the El Nino event. A similar ambiguity exists for the 1993 El Nino event, however, in this case it involves the vernal and autumnal Equinox spring tidal sequences. This ambiguity is resolved in a similar manner

Recall that figure 14 and table 1 show that the strongest spring tides that are closest to the date of the nominal Vernal equinox naturally break up into five distinct 31-year epochs that start in 1870, 1901, 1932, 1963 and 1994. Further recall that since the epochs that start in 1870, 1932, and 1994 begin with a Perigean Full moon, they are designated as Full Moon epochs, and that since the remaining two epochs that start in 1901 and 1963 begin with a Perigean New moon, they are designated as New Moon epochs. These boundary years are highlighted in figures 17 and 18 using vertical dashed lines.

Table 3:

Year El Nino	Starting Month	Date El Nino	E/S	Tidal Peak-Before	Tidal Peak-After	Difference (Years)
Equinox						
1877	Apr	1877.25	E	1874.212	**1878.213**	+0.963
			S	**1876.473**	1880.474	-0.777
1888	Jun	1888.41	E	**1887.714**	1891.716	-0.696
			S	1885.976	**1889.977**	+1.567
1896	Aug	1896.58	E	**1895.717**	1899.718	-0.863
			S	1893.979	**1897.980**	+1.400
1899	Sep	1899.67	E	1895.717	**1899.718**	+0.048
			S	**1897.980**	1901.984	-1.690
Solstice						
1902	May	1902.33	E	**1901.219**	1905.220	-1.111
			S	**1901.984**	1905.986	-0.346
1905	Mar	1905.16	E	1901.219	**1905.220**	+0.060
			S	**1903.483**	1907.484	-1.677
1911	Dec	1911.91	E	1909.221	**1913.223**	+1.313
			S	**1911.486**	1915.487	-0.424
1918	Oct	1918.75	E	**1918.723**	1922.724	-0.027
			S	**1916.981**	1920.983	-1.766
1925	Sep	1925.67	E	1922.724	**1926.725**	+1.055
			S	**1924.984**	1928.985	-0.686
1930	Jul	1930.50	E	1926.725	**1930.727**	+0.227
			S	**1928.985**	1932.956	-1.515
Equinox						
1940/fl	Jan	1940.00	E	1936.220	**1940.226**	+0.226
			S	1937.964	**1941.965**	+1.965
1940	Dec	1940.91	E	**1940.226**	1944.227	-0.684
			S	1937.964	**1941.965**	+1.055
1957	May	1957.33	E	1953.729	**1957.731**	+0.401
			S	**1955.469**	1959.470/B	-1.861
Solstice						
1963	Aug	1963.58	E	**1963.232**	1967.233	-0.348
			S	1960.963	**1964.965**	+1.385
1965	Jun	1965.41	E	1963.232	**1967.233**	+1.823
			S	**1964.965**	1968.966	-0.445
1972	Jun	1972.41	E	**1971.235**	1975.236	-1.175
			S	**1972.968**	1976.969	+0.558
1977	Sep	1977.67	E	**1976.730**	1980.731	-0.940
			S	1974.470	**1978.471**	+0.801
1982	May	1982.33	E	**1980.731**	1984.733	-1.599
			S	1978.471	**1982.473**	+0.143
1986	Oct	1986.75	E	1984.737	**1988.734**	+1.984
			S	**1986.474**	1990.475	-0.276
1991	Jun	1991.41	E	1988.734	**1992.735**	+1.325
			S	1987.973	**1991.974**	+0.564
1993	Mar	1993.25	E	1989.709	**1993.710**	+0.460
			S	**1991.974**	1995.976	-1.276
Equinox						
1994/fl	Sep	1994.67	E	**1993.710**	1997.712	-0.960
			S	1991.976	**1995.976**	+1.306
1997	May	1997.33	E	1993.710	**1997.712**	+0.380
			S	**1995.976**	1999.971	-1.354
2002	Jun	2002.41	E	1999.212	**2003.213**	+0.803
			S	1999.471	**2003.979**	+1.569
2009	Jul	2009.50	E	2007.214	**2011.216**	+1.716
			S	**2009.477**	2013.478	-0.023
2015	Feb	2015.08	E	2011.216	**2015.217**	+0.137
			S	**2013.478**	2017.479	-1.602

[N.B. The El Nino events that have an (*) in column 2 are those events that just fall short of our selection criterion because they only last for three months. They have been included in Table 2 for completeness.]

Figure 17

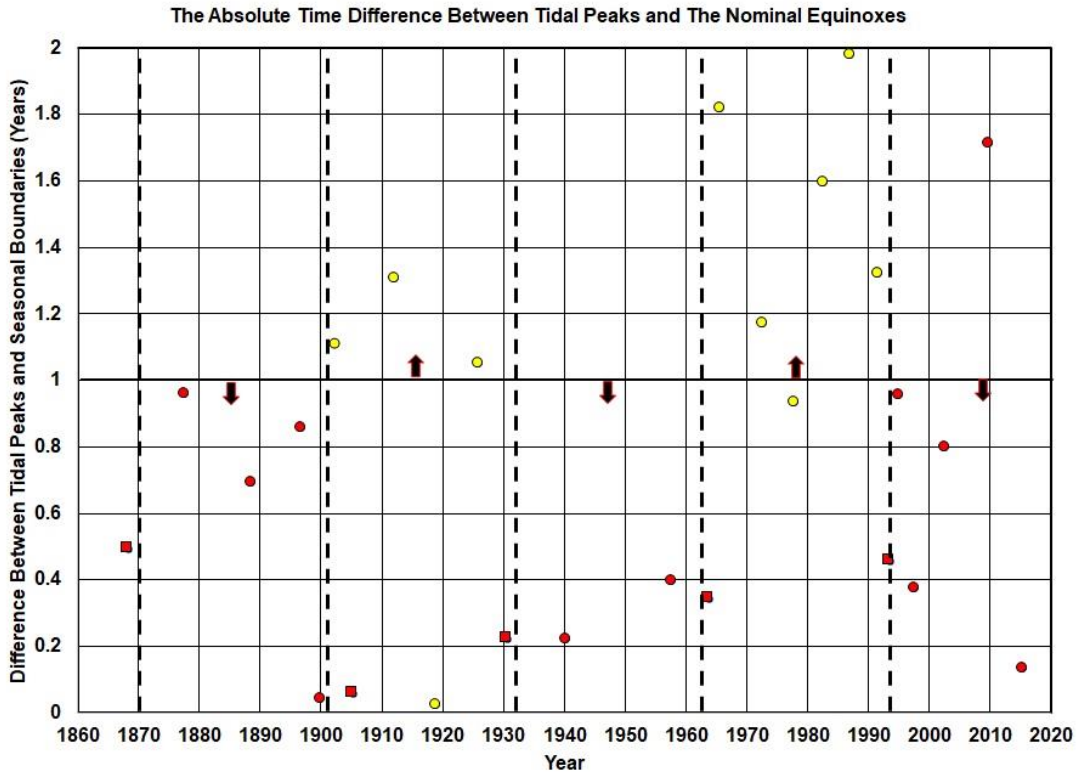

Figure 18

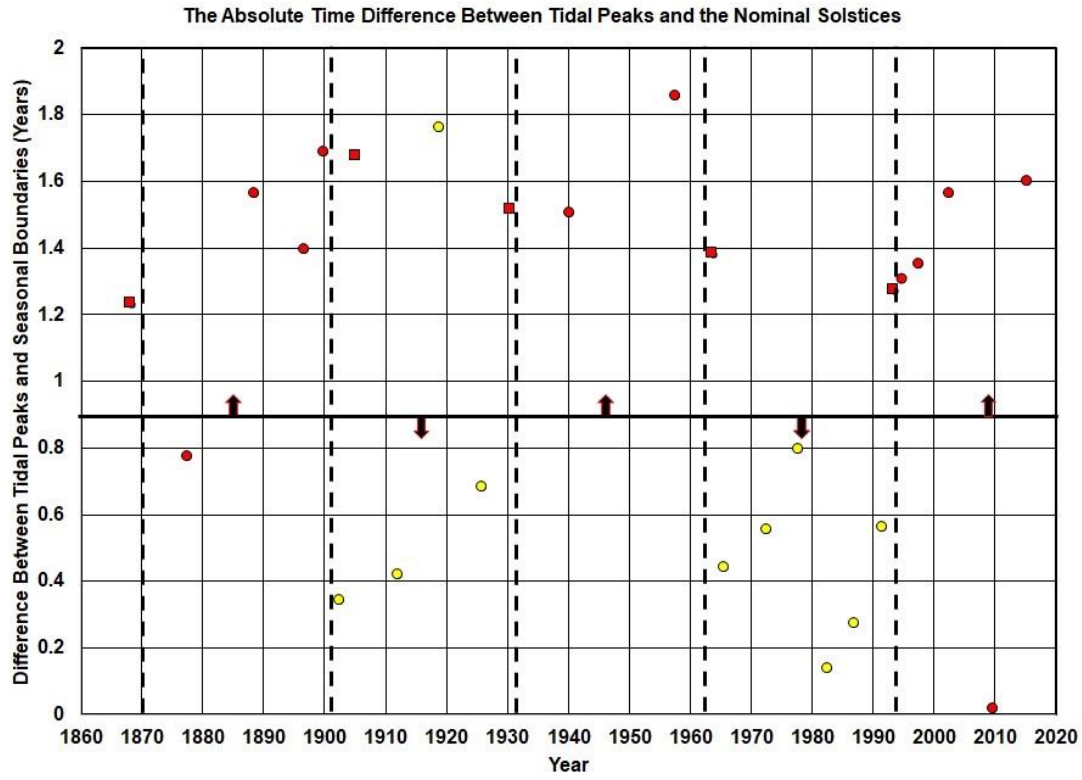

An inspection of figures 17 and 18 clearly show that the starting months of the El Ninos are best aligned with the Equinox spring tidal events during the Full moon epochs beginning in 1870, 1932, and 1994 (these points are plotted using red symbols), and best aligned with the Solstices spring tidal events during the New moon epochs beginning in 1901 and 1963 (these points are plotted using yellow symbols). However, there are four data points that are an exception to this general rule (i.e. those plotted as red squares in figures 17 and 18). These are the El Nino events that occur just before the start of the second, and third Full moon epochs in the years 1930, and 1993, and the El Nino events that occur just after the end of the first and second Full moon epochs, in the years 1905 and 1963.

Table 2 shows that the strongest spring tidal events exhibit a gradual (9-year) transition between one lunar epoch and the next. Interestingly, all four of the El Nino events that are an exception to the general rule occur in the 9.0-year transition periods that are associated with the start or end of a Full Moon epoch. This raises the possibility that the exceptional El Nino events are simply a consequence of the fact that one lunar tidal epoch is transitioning into the next. This would mean that they could be a part of the Full moon epoch even though they lie just outside the epochs boundaries.

Consequently, in the following analysis will consider two possible options. The first is that the four exceptional El Nino events are assumed to be associated with the Full Moon epochs (i.e. the "With Assumption" option), which can be considered as the most favourable case. The second is that the four exceptional El Nino events are assumed to be associated with the New Moon epochs (i.e. the "Without Assumption" option) which can be considered as the least favourable case.

Hence, given the two option being considered, there are two possible null hypothesis which can proven or disproven using a given a Chi-Squared test.

e) Using a Chi-Squared test to disprove the Null Hypothesis

The first null hypothesis ($H1_O$) assumes that all four exceptional El Nino events are a part of the Full Moon epochs, while the second null hypothesis ($H2_O$) assumes that all four exceptional El Nino events are a part of the New Moon epochs. Both null hypotheses propose that: The absolute time difference in years between the starting months of the El Ninos and

1) the times of Equinox spring tidal events during the Full moon epochs, AND
2) the times of Solstice spring tidal events during the New moon epochs,

randomly lies somewhere between 0.0 and 2.0 years. These null hypotheses should be true if there is no connection between the starting times for El Nino events and the times of Equinox or Solstice spring tidal events

Table 4a shows that, in the most favourable case, the likelihood that $H1_O$ is correct is $p < 0.0001$. This means that little doubt that we can reject the (first) null hypothesis ($\chi^2 = 21.692$, degrees of freedom (df) = 3). In like manner, table 4b shows that, in the least favourable case, the likelihood that $H2_O$ is correct is $p < 0.05$. This means that, even in the least favourable case (i.e. all four of the exceptional El Nino events are considered part of the New Moon epoch) we can reject the (second) null hypothesis ($\chi^2 = 7.846$, df = 3).

Hence, we can conclude that, even in the least favourable case, there is a distinct preference for El Nino events to start near the times when Equinox spring tidal events occur

Table 4a

χ^2 = 21.692 df =3 p<0.0001	With Assumption = The Most Favourable Case				
	0.00 to 0.50 yrs	0.50 to 1.00 yrs	1.00 to 1.50 yrs	1.50 to 2.00 yrs	Total Events
Equinox	9	6	0	1	16
Solstice	5	4	0	1	10
Combined	**14**	**10**	**0**	**2**	**26**
Expected	6.5	6.5	6.5	6.5	26

Table 4b

χ^2 = 7.846 df=3 p=0.05	Without Assumption = The Least Favourable Case				
	0.00 to 0.50 yrs	0.50 to 1.00 yrs	1.00 to 1.50 yrs	1.50 to 2.00 yrs	Total Events
Equinox	**5**	**6**	**0**	**1**	**12**
Solstice	**5**	**4**	**2**	**3**	**14**
Combined	**10**	**10**	**2**	**4**	**26**
Expected	**6.5**	**6.5**	**6.5**	**6.5**	**26**

during the Full Moon epochs and to start near the times when Solstice spring tidal events occur during New Moon epochs. This means that there must some connection between strongest Equinox/Solstice spring tidal events and the onset of El Nino events.

It is obvious, however, that the robustness of this claim is diminished to some degree by the small sample size. Indeed, it would only take one or two additional El Nino events that did not follow the observed pattern for p to exceed 0.05, rendering the result null and void for the least favourable case. Ideally, we will need a slightly larger sample size before we can feel more confident about this result.

5. Conclusions

Paper I showed that the epochs when the lunar line-of-apse points directly towards/away from the Sun, at times that were very close to Equinoxes and Solstices (i.e. seasonal boundaries), exhibited distinct periodicities at 28.75, 31.00, 88.50 (Gleissberg cycle), 148.25, and 208.00 (de Vries cycle) years. The caveat being that the alignments have to be observed in a frame of reference that was fixed with respect to the Perihelion of the Earth's orbit.

This study expands upon the findings of paper I by showing that the long-term periodicities exhibited by the alignments of the lunar line-of apse with the seasonal boundaries are effectively the same as the periodicities exhibited by the alignments of the Perigean New/Full moons with the seasonal boundaries (provided both are viewed in a frame of reference that was fixed with respect to the Perihelion of the Earth's orbit).

In addition, this study establishes that the very process of selecting the times when the Perigean New/Full moons occur at or near seasonal boundaries, is in effect equivalent to selecting the times when the strongest Perigean New/Full moon tidal events cross the Earth's equator or when they are at their furthest distance from the Earth's equator (i.e. lunar standstill).

Plots were made of the fractional part of a year versus the year for all the strongest spring tides that occurred between March 7th, 1860 and March 11th, 2030 that have tidal peaks which occur within ± 6^{O} of the Earth's equator. Effectively, this picks out the strongest spring tidal

events that occur close to the nominal Vernal Equinox (i.e. 0.00 UT March 21st) or close to the nominal Autumnal Equinox (i.e. 0.00 UT September 21st) that have peak tides at latitudes that are close to the Earth's equator. These plots show that the spring tidal events that are closest to the Vernal Equinox naturally divides into five 31-year epochs that start in the years 1870, 1901, 1932, 1963, and 1994. The three lunar tidal epochs that start in 1870, 1932, and 1994 begin with a Perigean Full moon, so they are designated as Full Moon epochs. Similarly, the remining two epochs that start in 1901 and 1963 begin with a Perigean New moon, so they are designated as New Moon epochs.

In addition, plots were made of the fractional part of a year versus the year for all the spring tides that occurred between December 1st, 1861 and December 14th, 2031 that have tidal that peak within 3^{O} of the latitude of the nearest lunar standstill. In effect, this picks out the strongest spring tidal events that occur close to the nominal Summer Solstice (i.e. 0.00 UT June 21st) or close to the nominal Winter Solstice (i.e. 0.00 UT December 21st) that have peak tides at latitudes that are close to those of the lunar standstills. These plots show that the spring tidal events that are closest to the Summer Solstice naturally divide into five 31-year epochs that start in the years 1872, 1903, 1934, 1965, and 1996.

Collectively, these plots show that the actual starting date for each of the 31-year epochs is dependent upon the seasonal boundary that is chosen. In addition, the data indicates that there is a gradual transition between one lunar epoch and the next that spans a 9.0-year period that is centred upon the time when the strongest spring tide is most closely align with the Spring Equinox.

Furthermore, we find that the times when strongest tidal peaks cross the Earth's equator [i.e. the Equinox spring tides, which are the strongest spring tidal events that are nearest to the times of the nominal Equinoxes] or the times when the strongest peaks reach their greatest distances from the Equator [i.e. the Solstice spring tides, which are the strongest spring tidal events that are nearest to the times of the nominal Solstices], correspond to the times when the lunar-induced rotational acceleration of the Earth changes sign. This leads to the question, can these lunar induced changes in the sign of the Earth's rotational acceleration be link to an atmospheric/oceanic phenomenon that is known to influence changes in the Earth's global mean temperature? Further investigate shows that the phenomenon that meets these requirements is the starting dates for moderate to strong El Nino events.

If a comparison is made between the starting dates for moderate to strong El Nino events and the times when the strongest spring tides are near to the Earth's equator [i.e. Equinox spring tides], there is an alignment between the two phenomena during Full Moon epochs (i.e. those starting in 1870, 1932, and 1994). Similarly, if a comparison is made between the starting dates for moderate to strong El Nino events and the times when the strongest spring tides are at their furthest distance from the Earth's equator [i.e. Solstice spring tides], there is an alignment during the New Moon epochs (i.e. those starting in 1901 and 1963).

Thus, we can conclude that, during the Full Moon epochs, there is a significant alignment between the starting dates of moderate to strong El Ninos and the times when Equinox spring tidal events occur. In addition, we can conclude that, during New Moon epochs, there is a significant alignment between the starting dates of moderate to strong El Ninos and the times when Solstice spring tidal events occur. This means that there must be a connection between the times of strongest Equinox/Solstice spring tidal events and the onset of El Ninos.

ACKNOWLEDGMENTS

One of the authors (IW) would like to acknowledge and celebrate the life of a truly great scientists, teacher and mentor Prof. Michael A. Dopita (MSSSO/ANU), who passed away in December 2018. His warmth, intellect, generosity and wisdom will be sorely missed.

CONFLICT OF INTEREST

No outside funding was used to conduct this work. No conflicts of interest are involved.

References:

Abreu, J.A., Beer, J., Ferriz-Mas, A., McCracken, K.G. and Steinhilber, F., **2012**, *Is there a planetary influence on solar activity?* Astron. & Astrophys., 548, A88.

Bromberg, I, **2016**, *The length of seasons (on Earth)*, http://www.sym454.org/seasons : last accessed 23/01/2019

Chapront-Touz, M. and Chapront, J., **1991**, *Lunar tables and programs from 4000 B. C. to A. D. 8000*. Willmann-Bell, Richmond VA; ISBN 0-943396-33-6

Damon, P.E., and Sonnet, C. P., **1991**, *The sun in time (A92-46664 19-92)*. Edited by Sonnet C.P., Giampa, M.S., and Matthews, M.S., Tucson, AZ, University of Arizona Press, p. 360-388; ISBN 0-8165-12987-3

Gleissberg, W., **1944**, *A table of secular variations of the solar cycle*, Terrestrial Magnetism and Atmospheric Electricity, 49, pp. 243–244, doi:10.1029/TE049i004p00243

GreenwichMeanTime.com, **2019**, *Soltices and Equinoxes 2010 – 2019*, https://greenwichmeantime.com/longest-day/equinox-solstice-2010-2019/

Laken, B.A., Kniveton, D.R., and Frogley, M.R., **2010**, *Cosmic rays linked to rapid mid-latitude cloud changes*, Atmos. Chem. Phys., 10, 10941–10948.

Marshall, J. and Plumb R. A., **2008**, *Atmosphere, Ocean and Climate Dynamics: An Introductory Text: Volume 93 of the International Geophysics Series*, Elsevier Academic Press.

McCracken, K.G., Beer, J., Steinhilber, F., and Abreu J., **2013**, *A Phenomenological Study of the Cosmic Ray Variations over the Past 9400 Years, and Their Implications Regarding Solar Activity and the Solar Dynamo*, Solar Physics, Vol. 286, 2, pp. 609-627.

Meeus, J., **1988**, *Astronomical Formula for Calculators, Fourth Edition*. Richmond: Willmann-Bell, ISBN 0-943396-22-0.

Meeus, J., **1998**, *Astronomical Algorithms*. Richmond: Willmann-Bell, ISBN 0-943396-63-8.

Nef, U., Burns, S.J., Mangini, A., Mudelsee, M., Fleitmann, D., and Matter, A., **2001,** *Strong coherence between solar variability and the monsoon in Oman between 9 and 6 kyr ago*, Nature, volume 411, pp. 290–293 (17 May).

NOAA **2019**a, http://www.cpc.ncep.noaa.gov/data/indices/soi

NOAA **2019b**: http://www.cpc.ncep.noaa.gov/data/indices/sstoi.indices

Peristykh, A.N. and Damon, P.E., **2003**, *Persistence of the Gleissberg 88-year solar cycle over the last 12,000 years: Evidence from cosmogenic isotope,* Journal of Geophysical Research, Vol. 108, No. A1, p 1003, doi:10.1029/2002JA009390

Ray, R.D. and Cartwright, D.E., **2007**, *Times of peak astronomical tides*, Geophys. J. Int., 168, 999–1004.

Ron, C., Chapanov, Y., and Vondrak, J., **2012**, *Solar Excitation of Bicentennial Earth Rotation Oscillations*, Geomater., Vol. 9, No. 3 (167), 259–268.

Salzer, M.W. and Kipfmueller, K.F., **2005**, *Reconstructed temperature and precipitation on a millennial timescale from tree-rings in the Southern Colorado Plateau U.S.A.* Climatic Change, 70, No 3, 465–487.

Simon, J.L., Bretagne, P., Chapront-Touzé, M., Francou, G., and Lasker, J., **1994**, "*Numerical Expressions for precession formulae and mean elements for the Moon and planets*". Astron. Astrophys. 282 (2), p. 669.

Smith, C.A. and P. Sardeshmukh, **2000**, *The Effect of ENSO on the Intraseasonal Variance of Surface Temperature in Winter*., International J. of Climatology, **20** 1543-1557.

Smith, C.A. and P. Sardeshmukh, **2018a**, http://www.esrl.noaa.gov/psd/people/cathy.smith/best/

Smith, C.A. and P. Sardeshmukh, **2018b**, http://www.esrl.noaa.gov/psd/people/cathy.smith/best/details.html

Smith, C.A. and P. Sardeshmukh, **2018c**, http://www.esrl.noaa.gov/psd/people/cathy.smith/best/table.txt

Smith, C.A. and P. Sardeshmukh, **2018d**, http://www.esrl.noaa.gov/psd/people/cathy.smith/best/table33.txt

Svensmark, H., **1998**. *Influence of cosmic rays on the earth's climate*. Phys. Rev. Lett. 81, 5027-3030.

Svensmark, H., **2007**. *Cosmoclimatology: a new theory emerges*. Astronomy & Geophysics. Blackwell Publishing. 48 (1): 18–24.

